



# The Landscape of Phenotypic and Transcriptional Responses to Ciprofloxacin in *Acinetobacter baumannii*: Acquired Resistance Alleles Modulate Drug-Induced SOS Response and Prophage Replication

Edward Geisinger,<sup>a,c</sup> Germán Vargas-Cuebas,<sup>a\*</sup> Nadav J. Mortman,<sup>a</sup> Sapna Syal,<sup>a</sup> Yunfei Dai,<sup>c</sup> Elizabeth L. Wainwright,<sup>c</sup> David Lazinski,<sup>a</sup> Stephen Wood,<sup>b</sup> Zeyu Zhu,<sup>b</sup> Jon Anthony,<sup>b</sup> Tim van Opijnen,<sup>b</sup> Ralph R. Isberg<sup>a</sup>

<sup>a</sup>Department of Molecular Biology and Microbiology, Tufts University School of Medicine, Boston, Massachusetts, USA

<sup>b</sup>Department of Biology, Boston College, Chestnut Hill, Massachusetts, USA

<sup>c</sup>Department of Biology, Northeastern University, Boston, Massachusetts, USA

**ABSTRACT** The emergence of fluoroquinolone resistance in nosocomial pathogens has restricted the clinical efficacy of this antibiotic class. In *Acinetobacter baumannii*, the majority of clinical isolates now show high-level resistance due to mutations in *gyrA* (DNA gyrase) and *parC* (topoisomerase IV [topo IV]). To investigate the molecular basis for fluoroquinolone resistance, an exhaustive mutation analysis was performed in both drug-sensitive and -resistant strains to identify loci that alter ciprofloxacin sensitivity. To this end, parallel fitness tests of over 60,000 unique insertion mutations were performed in strains with various alleles in genes encoding the drug targets. The spectra of mutations that altered drug sensitivity were found to be similar in the drug-sensitive and *gyrA parC* double-mutant backgrounds, having resistance alleles in both genes. In contrast, the introduction of a single *gyrA* resistance allele, resulting in preferential poisoning of topo IV by ciprofloxacin, led to extreme alterations in the insertion mutation fitness landscape. The distinguishing feature of preferential topo IV poisoning was enhanced induction of DNA synthesis in the region of two endogenous prophages, with DNA synthesis associated with excision and circularization of the phages. Induction of the selective DNA synthesis in the *gyrA* background was also linked to heightened prophage gene transcription and enhanced activation of the mutagenic SOS response relative to that observed in either the wild-type (WT) or *gyrA parC* double mutant. Therefore, the accumulation of mutations that result in the stepwise evolution of high ciprofloxacin resistance is tightly connected to modulation of the SOS response and endogenous prophage DNA synthesis.

**IMPORTANCE** Fluoroquinolones have been extremely successful antibiotics due to their ability to target multiple bacterial enzymes critical to DNA replication, the topoisomerases DNA gyrase and topo IV. Unfortunately, mutations lowering drug affinity for both enzymes are now widespread, rendering these drugs ineffective for many pathogens. To undermine this form of resistance, we examined how bacteria with target alterations differentially cope with fluoroquinolone exposures. We studied this problem in the nosocomial pathogen *A. baumannii*, which causes drug-resistant life-threatening infections. Employing genome-wide approaches, we uncovered numerous pathways that could be exploited to raise fluoroquinolone sensitivity independently of target alteration. Remarkably, fluoroquinolone targeting of topo IV in specific mutants caused dramatic hyperinduction of prophage replication and enhanced the mutagenic DNA damage response, but these responses were muted in strains with DNA gyrase as the primary target. This work demonstrates that resis-

**Citation** Geisinger E, Vargas-Cuebas G, Mortman NJ, Syal S, Dai Y, Wainwright EL, Lazinski D, Wood S, Zhu Z, Anthony J, van Opijnen T, Isberg RR. 2019. The landscape of phenotypic and transcriptional responses to ciprofloxacin in *Acinetobacter baumannii*: acquired resistance alleles modulate drug-induced SOS response and prophage replication. mBio 10:e01127-19. <https://doi.org/10.1128/mBio.01127-19>.

**Editor** Samuel I. Miller, University of Washington

**Copyright** © 2019 Geisinger et al. This is an open-access article distributed under the terms of the [Creative Commons Attribution 4.0 International license](https://creativecommons.org/licenses/by/4.0/).

Address correspondence to Ralph R. Isberg, [ralph.isberg@tufts.edu](mailto:ralph.isberg@tufts.edu).

\* Present address: Germán Vargas-Cuebas, Department of Microbiology and Immunology, Emory University School of Medicine, Atlanta, Georgia, USA.

**Received** 2 May 2019

**Accepted** 8 May 2019

**Published** 11 June 2019

tance evolution via target modification can profoundly modulate the antibiotic stress response, revealing potential resistance-associated liabilities.

**KEYWORDS** *Acinetobacter*, DNA gyrase, fitness, fluoroquinolone, prophage, antibiotic resistance, ciprofloxacin, topoisomerase IV

**A***cinetobacter baumannii* is a frequent cause of multidrug-resistant infections in hospitals and has been labeled a pathogen of critical priority for new drug development (1). This pathogen class has rapidly evolved a broad array of drug resistance mechanisms, limiting the usefulness of many widely used antibiotics. A prime example is the fluoroquinolone class of antibiotics. These drugs are widely used to treat infections caused by a range of Gram-negative and Gram-positive bacteria, but they have been rendered obsolete against most *A. baumannii* isolates due to extremely high frequencies of resistance (2–4). An understanding of how *A. baumannii* and related bacteria withstand treatment with fluoroquinolone antibiotics has the potential to lead to strategies to reverse or bypass resistance.

Fluoroquinolones inhibit DNA replication in bacteria by targeting two enzymes essential for DNA synthesis, the type II topoisomerase DNA gyrase (*gyrAB* genes) and topoisomerase IV (topo IV; *parCE*). These enzymes modulate DNA topology to maintain negative DNA supercoiling (DNA gyrase) or decatenate newly replicated DNA (topo IV), and in so doing, they break and religate DNA. Binding of fluoroquinolones to these enzymes traps them in an intermediate state that is bound to cleaved DNA, resulting in double-strand DNA breaks, blocked replication fork progression, and, at high drug concentrations, cell death (5).

Acquired resistance to fluoroquinolones commonly arises through stepwise mutations that disrupt the ability of the drug to bind its preferred target enzymes. In Gram-negative bacteria, including *A. baumannii*, these mutations typically arise first in *gyrA*, which encodes the GyrA subunit of DNA gyrase, the more sensitive of the two enzyme targets (6). In the presence of resistant GyrA, the less-sensitive topo IV (encoded by *parC*) becomes the target and the site of second-step resistance mutations. In addition to target site alterations, acquisition of mutations that upregulate drug efflux pumps or accessory genes that allow drug modification enable bacteria to develop fluoroquinolone resistance (7). A large fraction of *A. baumannii* isolates harbor target site mutations in *gyrA* and *parC* (8, 9) and mutations causing overproduction of one or more resistance-nodulation-division (RND) class efflux systems that act on fluoroquinolone drugs (AdeABC, AdeFGH, and/or AdeIJK [10–12]).

Acquired resistance mechanisms generally act in combination with intrinsic resistance strategies in a cumulative manner to raise the amount of fluoroquinolone antibiotic required to block bacterial growth. Regulated production of native efflux pumps contributes to intrinsic fluoroquinolone resistance in many bacteria (13). Of the RND systems in *A. baumannii*, native levels of AdeIJK in wild-type (WT) strains lacking acquired mutations have been shown to provide intrinsic resistance to fluoroquinolones (12). Whether regulated production of other efflux systems provides intrinsic fluoroquinolone resistance is less clear.

Another major strategy for intrinsic fluoroquinolone resistance is the activation of DNA damage repair pathways (14). DNA lesions caused by fluoroquinolone intoxication are processed to single-stranded DNA and subsequently induce the SOS repair response, resulting in derepression of many genes involved in DNA recombination, repair, and mutagenesis (15). Knockout mutations in a variety of DNA repair genes result in increased fluoroquinolone susceptibility in several species (14–24). In certain cases, the SOS response also induces mobile genetic elements that carry antibiotic resistance or toxin genes, potentially influencing the spread of resistance or virulence traits (25). The *A. baumannii* SOS repair response is noncanonical, lacking clear orthologs of many major players in other systems (26), and is characterized by a phenotypically variable response within cell populations (27). Inactivation of RecA, a central protein mediating DNA recombinational repair and SOS induction, or the RecBCD exonuclease V complex

**TABLE 1** MICs of ciprofloxacin with WT and mutant *A. baumannii* strains

Strain	Amino acid change for:		Ciprofloxacin MIC ( $\mu\text{g/ml}$ )
	GyrA	ParC	
ATCC 17978 (WT)			0.25
EGA336	S81L		2–4
GVA41		S84L	0.25
GVA37	S81L	S84L	32

responsible for double-strand-break repair, greatly raises fluoroquinolone sensitivity in *A. baumannii* (28, 29). The role of the SOS response and other DNA repair systems, however, in the development of antibiotic resistance in this organism is largely unknown.

As part of a large-scale effort to characterize the molecular nature of intrinsic resistance of *Acinetobacter baumannii* to antimicrobials, we identified the entire spectrum of transposon insertion mutations that cause altered sensitivity to the fluoroquinolone antibiotic ciprofloxacin during growth in bacteriological culture. A number of studies have demonstrated that mutations that cause antibiotic hypersensitization in strain backgrounds lacking demonstrable resistance loci exhibit these effects independently of whether there are target site resistance mutations or antibiotic-inactivating enzymes present in the strains being interrogated (20, 30). We wanted to test this model by first identifying, via transposon sequencing (Tn-seq), loci that confer intrinsic fluoroquinolone resistance in a strain background having intact drug targets and then comparing them with intrinsic resistance loci identified in strains having drug target mutations in *gyrA* and *parC*. This analysis led to the surprising discovery that the levels of SOS induction and endogenous prophage activation by fluoroquinolones show dramatic dependence on the drug target that is preferentially poisoned.

## RESULTS

**Identification of *Acinetobacter baumannii* loci that confer altered sensitivity to ciprofloxacin.** To identify genes in which insertion mutations resulted in altered sensitivity to ciprofloxacin, ciprofloxacin concentrations below the MIC (Table 1) were identified that resulted in growth rates of *A. baumannii* ATCC 17978 in rich broth that were between 60 and 80% of that observed without antibiotics, as determined by optical density (OD) measurements (Fig. 1A). With increasing drug concentration, there is also a decrease in CFU, which the OD measurements underestimate (see Fig. S1B in the supplemental material). Three of these ciprofloxacin concentrations were chosen for further analysis (0.05, 0.075, and 0.09 to 0.10  $\mu\text{g/ml}$ ) to determine the relative fitness of insertion mutations when subjected to each of the antibiotic stress conditions. Multiple independent Tn10 insertion pools (7 pools for 0.05  $\mu\text{g/ml}$  and 11 pools for 0.075 and 0.09 to 0.10  $\mu\text{g/ml}$  ciprofloxacin) having between 6,000 and 18,000 individual insertions (60,000 separate sites in all) were cultured in parallel in broth with or without ciprofloxacin for approximately 8 generations. DNA samples taken from the initial time point prior to growth ( $t_1$ ) and the final time point after 8 generations of growth ( $t_2$ ) were prepared from each of the pools. The insertion sites were then amplified preferentially and subjected to high-density sequencing, followed by determining the relative fitness of each insertion mutant based on the density of the reads (see Materials and Methods) (Data Set S1). Using accepted strategies, the fitness of each insertion mutant strain was calculated relative to the entire pool (31). To standardize the results across experiments, fitness values were normalized to insertions found in 18 neutral sites located in pseudogenes or endogenous transposon-related genes throughout the genome (“neutral” mutants), to allow an accurate quantitation of the representation of mutants relative to control insertions predicted to have no effect on growth (32). The normalized data from the individual insertion mutations were aggregated for each gene to calculate a mean fitness level for the entire spectrum of mutations found within a particular gene. The complete data sets were then displayed on an individual gene

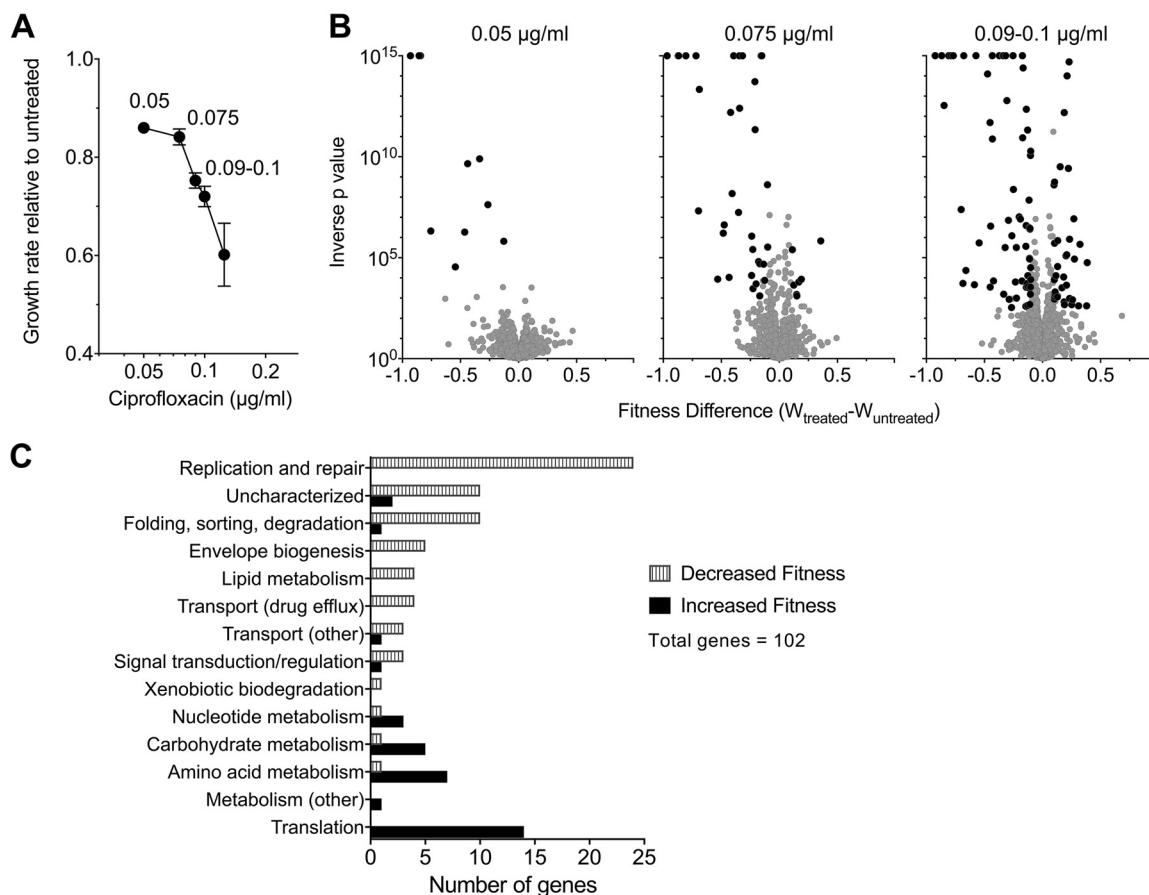


**FIG 1** Tn-seq quantification of genome-wide mutant fitness in *A. baumannii* ( $gyrA^{\text{WT}}$  and  $parC^{\text{WT}}$ ) during growth with sub-MIC ciprofloxacin. (A) Graded concentrations of ciprofloxacin cause increasing degrees of growth inhibition. Transposon mutant libraries constructed in a strain background harboring WT alleles of the *gyrA* and *parC* genes were grown with ciprofloxacin at the concentrations indicated. Growth rate relative to untreated control was determined from bacterial density measurements. Data points show average  $\pm$  SD ( $n \geq 2$ ). (B) Tn-seq fitness profiles during ciprofloxacin challenge. Mutant pools were grown with or without the indicated ciprofloxacin concentration, and the average fitness for each chromosomal gene was calculated. Change in fitness resulting from ciprofloxacin treatment relative to untreated controls is plotted against significance score resulting from parallel *t* tests. Data points shaded in black indicate gene knockouts causing significant alteration in fitness during drug challenge (magnitude of  $W_{\text{treated}} - W_{\text{untreated}}$   $> 0.1$ ; FDR,  $< 0.05$ ). (C) Functional categories of significant gene hits determining fitness during challenge with 0.09 to 0.1  $\mu\text{g/ml}$  ciprofloxacin. Information from KEGG and UniProt functional annotations and from orthologs in well-studied reference species were used to place genes into the listed broad categories.

level as the growth rate changes for mutations relative to the growth rate of the entire pool (Fig. 1B). Candidate mutants were identified that showed lower or higher fitness levels based on the criteria that the false-discovery rate (FDR)  $q$  value was  $< 0.05$ , the change in fitness ( $W_{\text{diff}}$ ) was  $> 10\%$ , and fitness value was derived from at least 3 independent insertion mutants (33) (see Materials and Methods). For this work, we refer to lesions resulting in lowered relative fitness during growth with ciprofloxacin as ciprofloxacin-hypersensitizing mutations, and we refer to the genes harboring these mutations as loci of hypersensitization.

Small increases in the dose of ciprofloxacin greatly increased the spectrum of ciprofloxacin hypersensitivity loci (Fig. 1B, black). At a dose causing approximately 15% growth inhibition, mutations in only 10 genes passed the criteria for lower fitness relative to the rest of the pool in the presence of the drug. These included insertions in two genes involved in double-strand-break repair (*recB* and *ruvA*, encoding subunits of exonuclease V and the Holliday junction helicase); the major egress pump which is often found overproduced in clinical strains having high-level fluoroquinolone resistance (*adeIJK*); and *ctpA*, a periplasmic protease shown to be a target of mutations that augment  $\beta$ -lactam resistance in strains lacking the *bfmRS* global regulatory system (34)

(Data Set S1). Increasing the drug dose had two effects on expanding the spectrum of hypersensitivity loci. First, although the number of hypersensitivity loci that contribute to the enzymology of DNA repair increased from 2 members to 20 in the high-dose regimen, this expansion largely involved hitting additional subunits of the same complexes or backup systems of the enzymes identified in the low-dose regimen (*recBCD*, *sbcCD*, and *ruvABC*) (Data Set S1). This emphasizes the importance of protecting against double-strand breaks caused by fluoroquinolone-poisoned DNA gyrase (35). Second, increasing the dose resulted in hypersensitivity loci in cell envelope integrity proteins, additional protein-processing enzymes, and a MATE class proton-driven efflux pump (*abeM*) shown to export ciprofloxacin and other antibiotic compounds when cloned in *Escherichia coli* (36) (Data Set S1 and Fig. 1C). Interestingly, increasing the drug dose did not implicate the two other major RND efflux systems in protecting from ciprofloxacin stress even though they are known to provide low-level resistance after overproduction (12). This may be explained by the fact that the *adeJJK* system is the only RND egress pump known to have a high basal level of expression in WT strains lacking acquired resistance mutations, while the inducing signals for the other systems have not been identified (12). Strikingly, at the higher drug doses, mutations in *adeN*, which encodes the negative regulator of *adeJJK*, increased the fitness of *A. baumannii* relative to the rest of the pool (Data Set S1). These data argue strongly that the primary efflux pumps involved in intrinsic protection from fluoroquinolone stress are AdelJK and AbeM.

In addition to hypersensitivity loci, mutations were identified at the highest drug dose that resulted in increased fitness relative to the insertion pool (Fig. 1B and C and Data Set S1). The mutations that most frequently increased fitness targeted nonessential components of the protein translation machinery, particularly enzymes that post-translationally modify tRNA, rRNA, and assembly of ribosomal protein complexes. That disruption of this circuit is being associated with increased drug resistance is consistent with studies showing that a spectrum of antibiotic-resistant isolates in different species evolve mutations that cause a lower translation rate (37, 38). The results are also consistent with a study demonstrating that lowering ribosomal synthesis increases resistance to ciprofloxacin by restoring an optimal balance between protein and DNA synthesis levels during DNA stress (39). Most notable among the insertions identified were those in *gidA*, which is part of a complex involved in 5-methylaminomethyl-2-thiouridine (mnm<sup>5</sup>s<sup>2</sup>U34) modification of tRNAs (Data Set S1) (40). We have previously identified this gene as an additional target of mutations bypassing drug hypersensitivity resulting from a loss of *bfmRS* (34), indicating the tight connection between mutations in this gene and drug resistance.

**Deletion mutants have drug sensitivities predicted by Tn-seq.** Targeted deletion mutations were constructed in nonessential genes predicted to have altered drug sensitivity in the presence of ciprofloxacin. The mutations were chosen based on their fitness in the Tn-seq analysis, the magnitude of the effects predicted, and differing functional categories (Fig. 1C). For instance, mutations in the egress pump-encoding *adeJJK* showed extremely poor fitness and were rarely recovered after growth in ciprofloxacin (Fig. 2A). Similarly, the insertions in *ctpA* showed very low fitness. In contrast, although ciprofloxacin treatment lowered fitness for mutants lacking the penicillin binding protein 1A (PBP1A), these mutations clearly had weaker effects in the Tn-seq analysis. When this set of targeted mutants was analyzed further, the loss of *adeJJK*, *recN*, and *ctpA* all resulted in heightened drug sensitivity, as measured by growth in broth with or without ciprofloxacin (Fig. 2B). A *pbp1A* knockout strain harboring a frameshift mutation (see Materials and Methods) also showed heightened drug sensitivity (Fig. 2B). In addition, we assessed the ability of the *ctpA* deletion strain to form colonies on solid medium containing graded levels of ciprofloxacin. At drug concentrations that were below the MIC for the WT, the *ctpA* deletion mutation resulted in lower colony formation efficiency, and this hypersensitivity phenotype could be rescued by the reintroduction of *ctpA* on a plasmid (Fig. 2C). In contrast to these

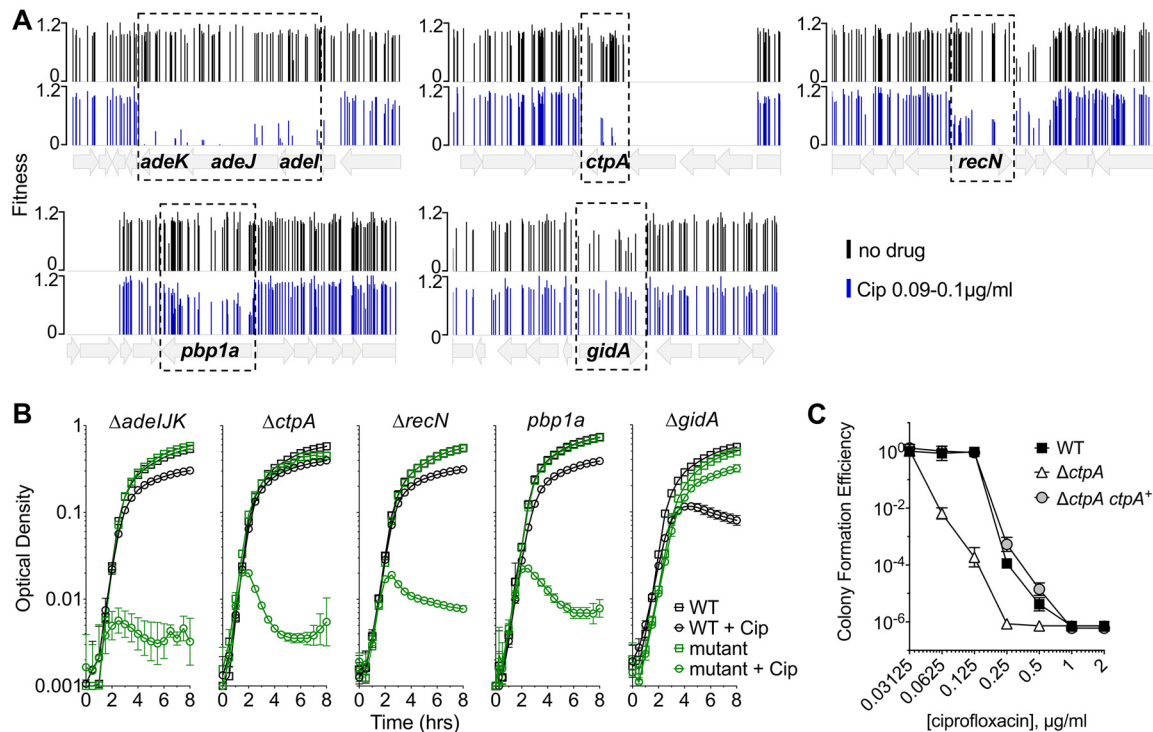


**FIG 2** Magnitude of growth impairment is predicted by the severity of the Tn-seq fitness defect. (A) Tn-seq fitness profiles of transposon mutant pools constructed in a *gyrA*<sup>WT</sup> *parC*<sup>WT</sup> mutant strain. Pools were grown without or with ciprofloxacin (Cip) at 0.09 to 0.1 μg/ml. Bars show fitness values of each transposon mutant at the indicated locus across all tested pools. (B) Growth of pure cultures of WT or the indicated mutant in the absence or presence of ciprofloxacin (0.09 μg/ml for  $\Delta ctpA$  and *pbp1a* mutants, 0.1 μg/ml for  $\Delta adeIJK$  and  $\Delta recN$  mutants, and 0.15 μg/ml for  $\Delta gidA$  mutant). The *pbp1a* mutant tested was *pbp1a*(N178TfsX27). Data points show geometric mean  $\pm$  SD ( $n = 3$ ). (C)  $\Delta ctpA$  mutant shows lowered efficiency of colony formation on ciprofloxacin medium. WT bacteria with control plasmid (pEGE244),  $\Delta ctpA$  mutant with control plasmid (pEGE244), and  $\Delta ctpA$  mutant with plasmid-borne *ctpA*(pGVE41) were grown on increasing concentrations of ciprofloxacin on solid LB agar medium. Data points represent the geometric mean  $\pm$  SD ( $n = 3$ ).

hypersensitivity loci, the deletion of *gidA*-encoded tRNA modification enzyme resulted in enhanced fitness in the presence of ciprofloxacin, with increased yields in broth cultures exposed to 0.15 μg/ml of antibiotic (Fig. 2B).

**Identification of loci that result in altered ciprofloxacin sensitivity in *A. baumannii* target site mutants.** Most of the current clinical isolates of *A. baumannii* are resistant to fluoroquinolones, and these isolates commonly have the *gyrA*(S81L) and *parC*(S84L) target site mutations that lower the affinity for these antibiotics (41). To determine the spectrum of insertions that cause altered sensitivity to ciprofloxacin in strains having resistance alleles, *gyrA*(S81L) (here referred to as *gyrA*<sup>r</sup>) and *gyrA*(S81L) *parC*(S84L) (referred to here as *gyrA*<sup>r</sup> *parC*<sup>r</sup>) mutants were generated, and each strain was subjected to Tn10 mutagenesis. Pools totaling more than 70,000 insertion mutations were constructed in each background. Insertion pools were challenged with ciprofloxacin, using drug concentrations below the MIC (Table 1) that resulted in 25 to 30% growth inhibition for each strain (1.1 μg/ml for the *gyrA*<sup>r</sup> mutant, 13 to 14 μg/ml for the *gyrA*<sup>r</sup> *parC*<sup>r</sup> double mutant; Fig. 3A). The spectrum of insertions that resulted in hypersensitivity to ciprofloxacin in the *gyrA*<sup>r</sup> *parC*<sup>r</sup> double-mutant strain backgrounds was very similar to that for the WT (Fig. 3C and D). In fact, almost every ciprofloxacin-hypersensitive locus in the double-mutant background was identified previously in the WT (Fig. 3C, green circles, and Data Sets S1 and S3). In addition, there was a number of hypersensitivity loci identified in the WT pools that did not pass the discovery criteria in the double mutant ( $FDR < 0.05$ ;  $W_{diff} > 0.1$ ). A number of these below-threshold candidates in the *gyrA*<sup>r</sup> *parC*<sup>r</sup> double-mutant strain background encoded subunits of the proteins identified as ciprofloxacin-hypersensitive loci (Fig. 3C, green circles, and Data Set S3). These results are similar to what we had observed in our graded series of

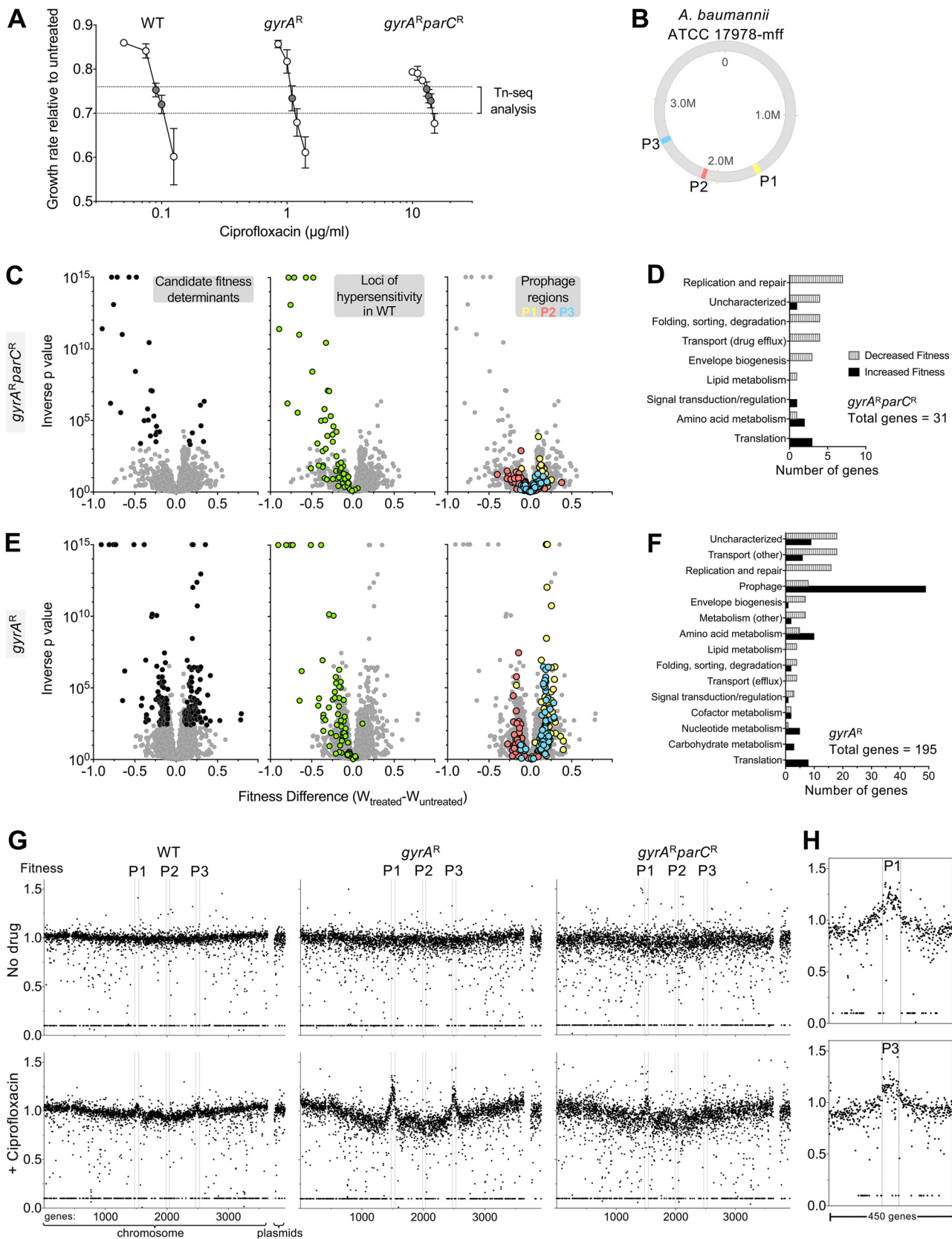


**FIG 3** Acquisition of *gyrA* resistance allele dramatically alters *A. baumannii* Tn-seq profile during ciprofloxacin challenge. (A) Transposon pools constructed in strains harboring resistance alleles in *gyrA* or both *gyrA* and *parC* require increasing concentrations of ciprofloxacin to result in growth inhibition. Growth rate inhibition relative to untreated pools based on bacterial density measurements was plotted as in Fig. 1A. *gyrA<sup>WT</sup> parC<sup>WT</sup>* mutant  
(Continued on next page)

drug treatments of insertion pools in the WT strain, indicating that the results from the WT strain and the drug-resistant double mutant are largely the same.

The results from the *gyrA*<sup>r</sup> single-mutant background, however, diverged greatly from those with the WT and the *gyrA*<sup>r</sup> *parC*<sup>r</sup> double mutant (Fig. 3E). A large fraction of insertions were identified that altered drug sensitivity to ciprofloxacin, with a surprising number showing increased fitness during drug exposure (Fig. 3E). Over 40 of the insertions that exhibited increased fitness were located in putative prophage genes (Fig. 3E and F, blue and yellow circles) from two of the three predicted phages integrated into the bacterial chromosome (Fig. 3B and Data Set S2). No such fitness changes were seen in the WT (Fig. S2 and Data Set S1) or *gyrA*<sup>r</sup> *parC*<sup>r</sup> double mutant (Fig. 3C and Data Set S3). To analyze this result further, the normalized fitness of mutations in each gene was plotted as a function of position on the chromosome. In the absence of antibiotic, there was no clear positional effect of altered fitness levels along the length of the chromosome (Fig. 3G). In contrast, in the presence of antibiotic, there was an apparent increase in fitness levels centered within chromosomal locations harboring prophages P1 and P3 in the *gyrA*<sup>r</sup> single mutant (Fig. 3G). Although some of this effect could be explained by a loss of prophage gene function resulting in enhanced fitness, insertions in chromosomal regions near, but outside, the prophage boundaries similarly showed apparent increases in fitness relative to the rest of the chromosomal insertions (Fig. 3G and H). As fitness levels are measured by counting the number of reads in specific regions of DNA, this phenomenon is consistent with selective local amplification of chromosomal material that initiates within these prophages, extending outward from the integration sites into nearby DNA regions. Deleting both P1 and P3 in the *gyrA*<sup>r</sup> background resulted in increased density during bacterial entry into postexponential phase in the presence of ciprofloxacin concentrations that approximate the MIC (Fig. S2B). This further supports the model that drug-induced amplification of prophage locus DNA was a major reason for heightened Tn-seq fitness values associated with transposons in these regions.

**Two prophage regions are selectively amplified in response to ciprofloxacin in the *gyrA*<sup>r</sup> single mutant.** As an additional test of the model that there is induction of DNA synthesis in the region surrounding two of the chromosomally located prophage clusters, we directly analyzed the chromosomal DNA content in the WT and *gyrA*<sup>r</sup> and *gyrA*<sup>r</sup> *parC*<sup>r</sup> mutant strains responding to drug treatment. Purified single colonies from each strain were grown in broth culture for 3.5 h in the presence of four different concentrations of ciprofloxacin that ranged from ~25 to 50% growth inhibition and compared to bacteria grown in the absence of drug (Fig. 4A). DNA was then prepared from each of the cultures and subjected to whole-genome sequencing using an average read length of 100 bp. The density of these individual short reads was plotted as a function of the chromosomal coordinates to identify regions of chromosomal DNA that were selectively amplified in the presence of drug (Fig. 4B). Analysis of the *gyrA*<sup>r</sup> single mutant showed hyperamplification of prophages P1 and P3, with read density in the prophage regions observed as a function of drug concentration. In contrast, there

### FIG 3 Legend (Continued)

growth data are from an identical experiment shown in Fig. 1A and are displayed to allow comparison to behavior of drug resistant mutants. Data points show average  $\pm$  SD ( $n \geq 2$ ). Samples from cultures with 25 to 30% growth inhibition (dotted lines) were processed for Tn-seq. (B) Location of prophage regions (P1 to P3) on *A. baumannii* 17978-mff chromosome map. Prophage positions were identified by using the PHASTER database (68). (C to F) *gyrA*<sup>r</sup> resistance allele influences Tn-seq fitness profiles associated with ciprofloxacin stress. Mutant pools were challenged with drug concentrations that resulted in equivalent 25 to 30% growth inhibition (*gyrA*<sup>r</sup> mutant, 1.1  $\mu$ g/ml; *gyrA*<sup>r</sup> *parC*<sup>r</sup> mutant, 13 to 14  $\mu$ g/ml). (C and E) Tn-seq fitness scores for each chromosomal gene with the indicated strain were calculated and visualized as in Fig. 1B (left). Middle and right graphs show the identical data set, with highlighting of loci for which knockout causes ciprofloxacin hypersensitization in the WT genetic background (green), or loci within prophages (color indicated in key). (D and F) Gene hits associated with significant changes in fitness during treatment were placed into functional categories as in Fig. 1C. (F) Tn-seq hits resulting from *gyrA*<sup>r</sup> mutant libraries treated with ciprofloxacin are enriched in prophage genes. (G) Tn-seq fitness scores resulting from ciprofloxacin challenge show genome positional bias that is greatly amplified in *gyrA*<sup>r</sup> mutant pools. Average per-gene Tn-seq fitness values are plotted in order of gene position on the chromosome or on plasmids pAB1 to pAB3. Boundaries of prophage regions (P1 to P3) are indicated by vertical dotted lines. Top, no-drug control. Bottom, ciprofloxacin was added at the concentrations indicated in panel A (WT, 0.09 to 0.1  $\mu$ g/ml; *gyrA*<sup>r</sup> mutant, 1.1  $\mu$ g/ml; *gyrA*<sup>r</sup> *parC*<sup>r</sup> mutant, 13 to 14  $\mu$ g/ml). (H) Expanded view of per-gene Tn-seq fitness scores in regions surrounding prophages P1 and P3 for *gyrA*<sup>r</sup> mutant treated with 1.1  $\mu$ g/ml ciprofloxacin.



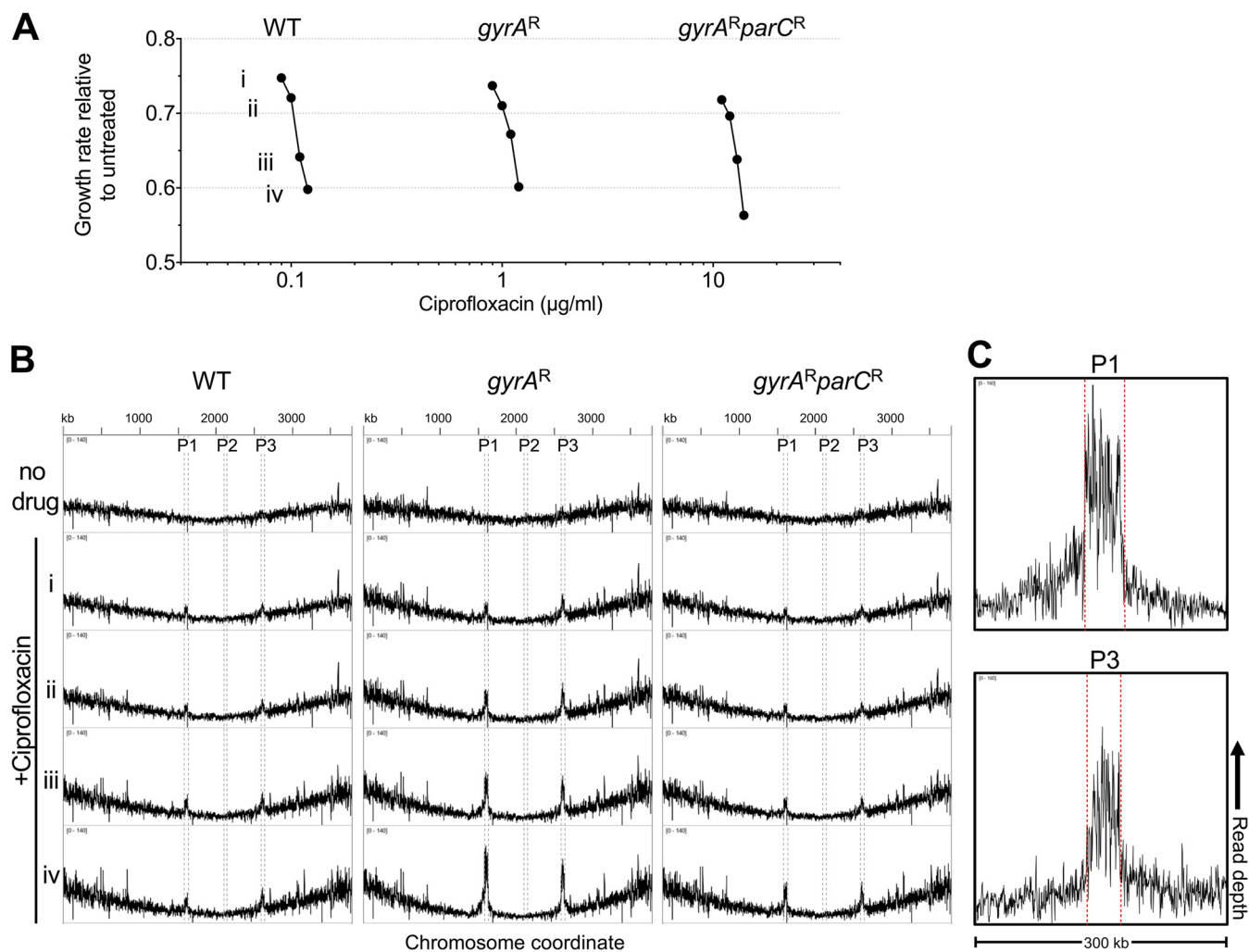


**FIG 4** Ciprofloxacin-induced amplification of prophage DNA in strains harboring the *gyrA<sup>r</sup>* single-step resistance genotype. (A) Pure cultures of strains of the indicated genotype were challenged with graded ciprofloxacin doses resulting in four levels of growth inhibition (Roman numerals). (B) DNA content from each culture was analyzed by deep sequencing. The x axis indicates nucleotide position along the *A. baumannii* ATCC 17978-mff chromosome. The y axis indicates normalized read depth (0 to 140 counts per million). Boundaries of prophage regions P1 to -3 are indicated by dashed lines. Roman numerals indicate the level of growth inhibition caused by ciprofloxacin. Data are representative of two independent experiments. (C) Expanded view of 300-kb window showing amplification of genomic regions surrounding prophages P1 and P3. The y axis indicates normalized sequencing read depth (0 to 160 counts per million).

was little evidence of this selective amplification in the WT strain, while the *gyrA<sup>r</sup> parC<sup>r</sup>* mutant largely reversed these effects. Consistent with the Tn-seq data, there was amplification of DNA extending beyond the prophage-chromosomal DNA junction, indicating that drug-driven DNA synthesis was initiated *in situ* and continued beyond the ends of the prophages into adjacent chromosomal DNA (Fig. 4C). In addition to this apparent *in situ* DNA amplification, P1 and P3 excision and phage genome circularization could be detected. To measure circularization and excision, the presence of *attB* and *attP* loci, which are absent in the intact prophage, was identified and quantified in the sequencing reads (Fig. 5A and B). Excision and circularization were detected at frequencies that increased with increasing drug dose in the *gyrA<sup>r</sup>* strain (Fig. 5C). Strikingly, increasing drug concentrations also resulted in an excess of *attP* copies relative to *attB* (Fig. 5C), consistent with replication of circular phage genomes and excision from the chromosome. In contrast, the efficiency of such events was muted or close to background in either the WT or the *gyrA<sup>r</sup> parC<sup>r</sup>* backgrounds (Fig. 5C). We conclude that in a *gyrA<sup>r</sup>* background, selective blockage of the *parC*-encoded topoisomerase IV protein resulted in DNA synthesis induction and phage genome multiplication in these two prophage regions.

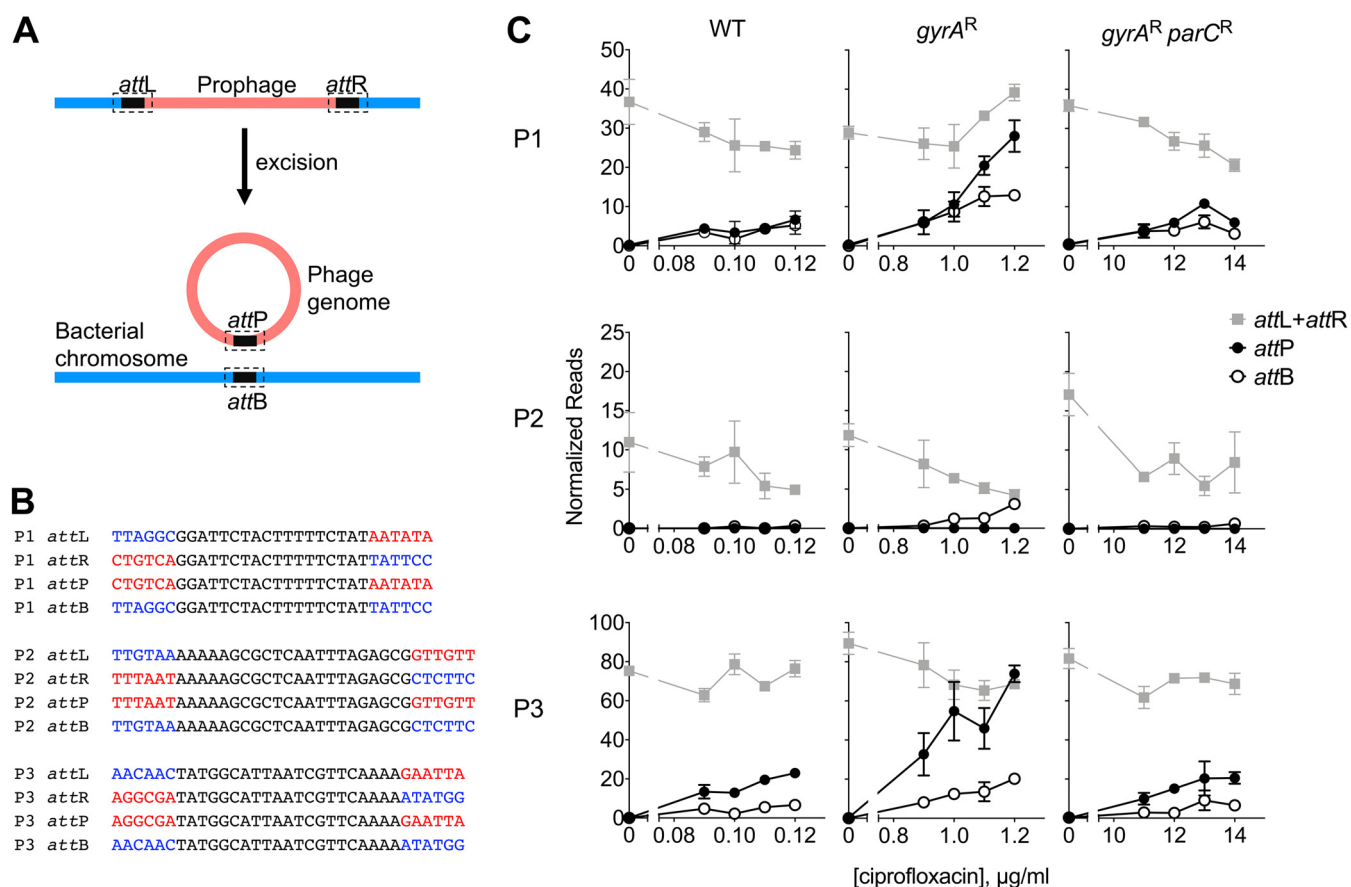


**FIG 5** Enhanced frequency of prophage excision and circularization in *gyrA*<sup>r</sup> single mutant. (A) Diagram of prophage excision at attachment sites (*att*; indicated by dashed boxes) showing generation of *attP* and *attB* sites after excision. (B) Prophage core *att* sequences (black) were determined using PHASTER database and BLAST analysis. Six-base-arm sequences flanking the core *att* sites were used to define *attL*, *attR*, *attP*, and *attB*. Prophage-specific DNA is shown in red, and chromosome-specific DNA is shown in blue. (C) Illumina whole-genome sequencing reads from experiment shown in Fig. 4 and an additional independent experiment were searched using the sequences shown in panel B. Read counts were normalized against total library size and displayed as counts per 10 million reads. Data points show average of normalized read count  $\pm$  range ( $n = 2$ ).

To determine if the transcription of prophage genes is specifically amplified in the *gyrA*<sup>r</sup> mutant relative to the WT, the two strains were grown in triplicate cultures in two concentrations of antibiotic for 3.5 h that gave between 30 and 40% growth inhibition over approximately 7 generations (Fig. 6A). The cells were then extracted and subjected to RNAtag-seq analysis (42), and the ratio of transcription for each gene in the presence/absence of ciprofloxacin was displayed as a function of chromosomal map position (Fig. 6B and Data Set S4). There was preferential amplification of transcription of prophage genes in the presence of antibiotic treatment in both strain backgrounds (Fig. 6B). Furthermore, transcription was hyperactivated in all three prophages, including prophage 2, which showed no evidence of preferential DNA amplification (compare Fig. 4B and 6B). A high proportion of genes in all three prophages showed transcriptional responses to ciprofloxacin that were significantly higher in the *gyrA*<sup>r</sup> single mutant than in the WT (Fig. 6B and S3). In *gyrA*<sup>r</sup> single mutants, enhanced expression in response to ciprofloxacin extended beyond the prophage-chromosomal DNA junctions with prophage 1 and, to some extent, with prophage 3 (Fig. 6C), consistent with increased DNA template availability partially contributing to heightened transcription in this strain background. Hyperexpression in response to ciprofloxacin terminated at the prophage-chromosomal DNA junctions with prophage 2, consistent with the observation that this region experienced no DNA amplification (Fig. 6C). These results indicate that preferential blockage of topo IV in the single mutant results in hyperactivation of prophage transcripts.

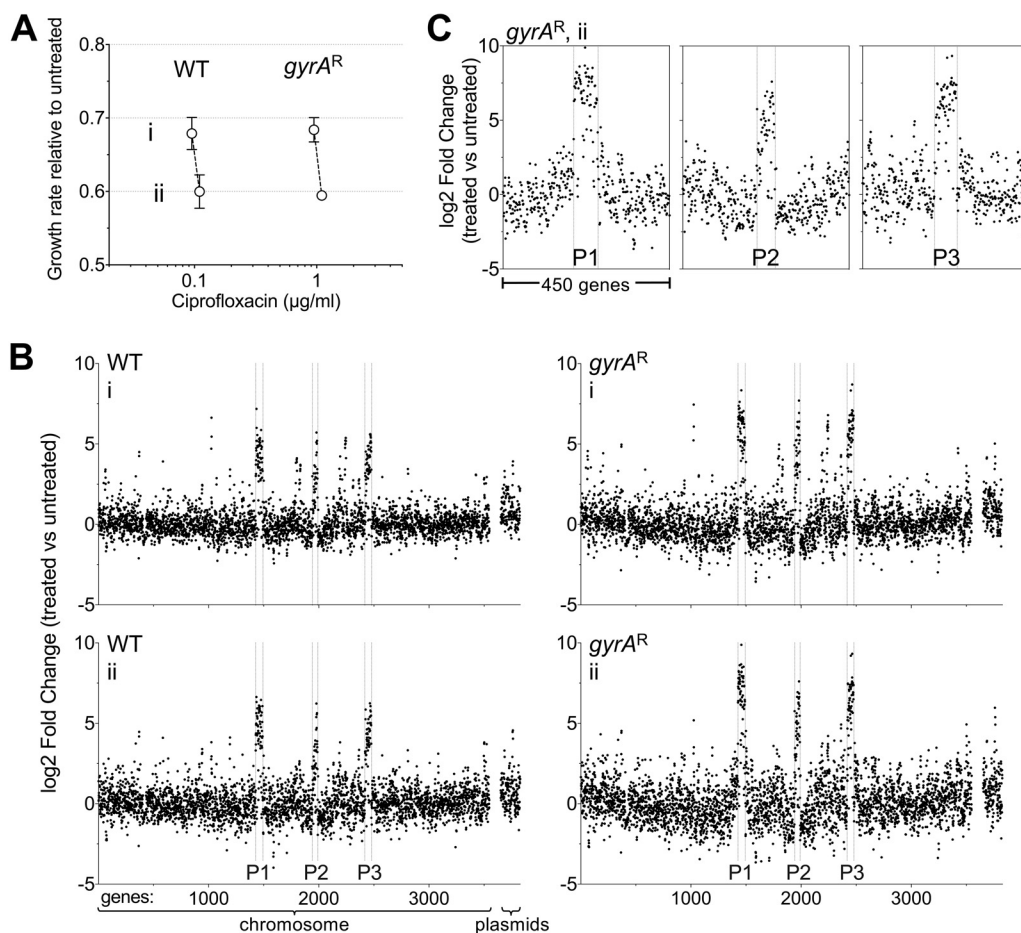


**FIG 6** Ciprofloxacin challenge results in activation of prophage gene expression that is heightened in *gyrA<sup>R</sup>* single mutants. (A) Strains of the indicated genotype were challenged with ciprofloxacin concentrations that resulted in two levels of growth inhibition relative to no treatment (i, ~30% growth inhibition; ii, ~40% growth inhibition). Data points show average  $\pm$  SD ( $n = 3$ ). (B) RNA-seq transcriptional profiles of cultures in panel A. Fold change ( $\log_2$ ) of each gene (treated versus untreated) was plotted in order of position on the chromosome or plasmids (pAB1 to pAB3). rRNA and tRNA genes were excluded from RNA-seq analysis, resulting in different gene number assignments from those in Fig. 3G. Boundaries of prophage regions P1 to P3 are denoted by vertical dotted lines. Roman numerals indicate growth inhibition level. (C) Expanded views of RNA-seq  $\log_2$  fold change ratios for genes surrounding P1 to P3 in *gyrA<sup>R</sup>* single mutant (condition ii, 1.1  $\mu$ g/ml ciprofloxacin).

### Ciprofloxacin-induced SOS response is selectively enhanced in the *gyrA<sup>R</sup>* single mutant.

Intoxication of bacterial topoisomerase enzymes by fluoroquinolone antibiotics induces DNA damage, driving an SOS response (16, 43). We investigated the extent to which ciprofloxacin-induced hyperactivation of prophage gene expression coincided with SOS response induction and whether the *gyrA* and *parC* resistance alleles influenced this response. Several genes associated with the SOS response (27, 43, 44) showed heightened transcription as a consequence of ciprofloxacin treatment (Fig. 7A). For several SOS genes, induction of transcripts was significantly higher in the *gyrA<sup>R</sup>* mutant than in the WT (Fig. 7A, asterisks). These included genes adjacent to prophage-chromosomal DNA junctions (*umuC* and *umuD* paralogs) as well as those not linked to prophages (*recA* and *gst*; Fig. 7B). RecA is a key component of the SOS response that is induced by DNA damage in *A. baumannii* and is critical for withstanding ciprofloxacin stress independent of the background resistance genotype (see Data Sets S1 to S3). To analyze the interplay of SOS induction by ciprofloxacin with target availability at the level of single cells, we utilized a plasmid-based transcriptional fusion of the *recA* regulatory elements (promoter and 5'-untranslated region [5'-UTR]) to the fluorescent reporter *mKate2* (45). WT, *gyrA<sup>R</sup>* mutant, and *gyrA<sup>R</sup> parC<sup>R</sup>* mutant strains harboring the

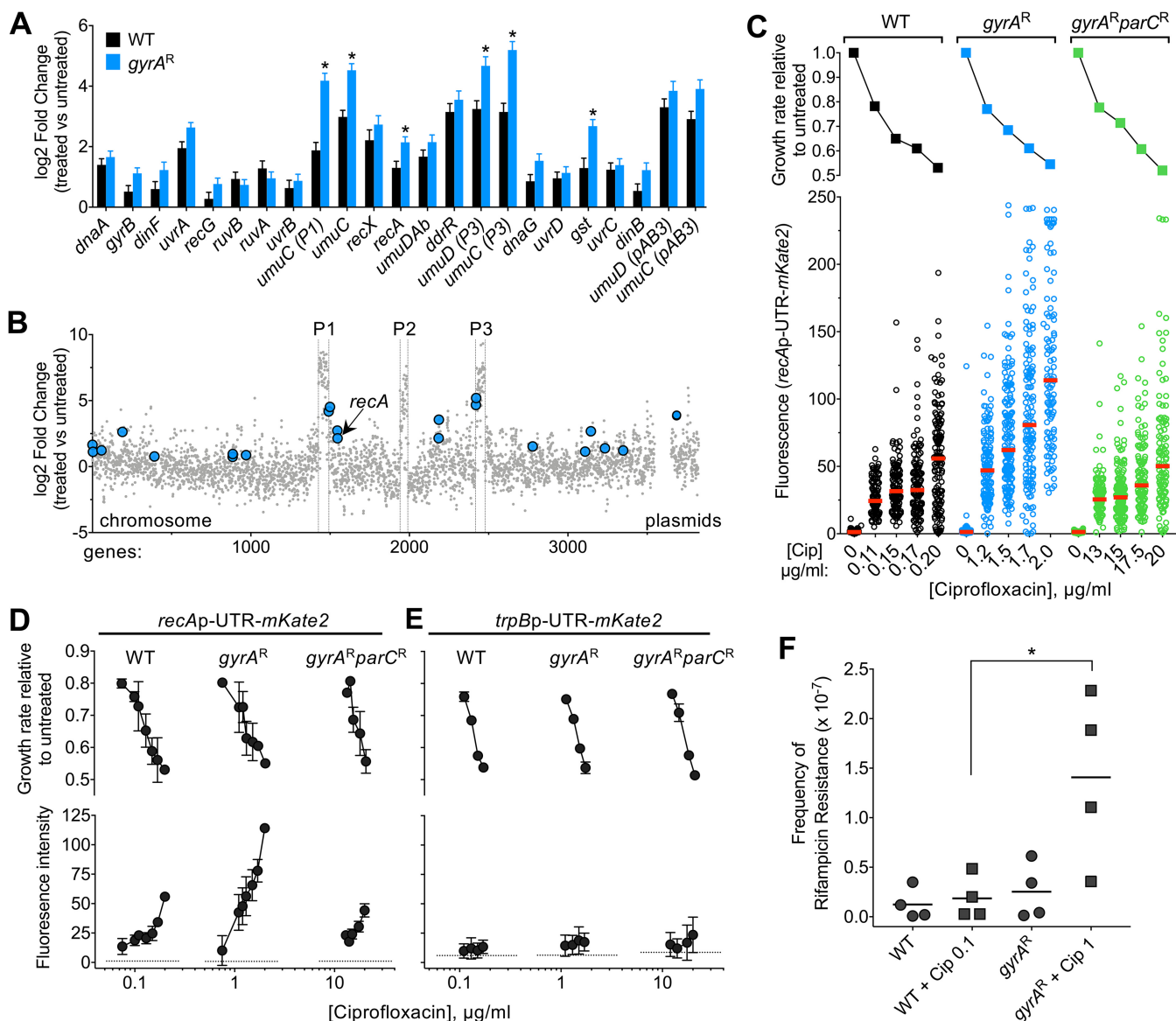


**FIG 7** Enhanced SOS response induction in *gyrA*<sup>r</sup> single mutants exposed to sub-MIC ciprofloxacin. (A and B) SOS response genes are induced during growth with ciprofloxacin. (A) RNA-seq data reveal DNA damage/SOS response induction during growth with ciprofloxacin. Bars show log<sub>2</sub> fold change ± SEM (n = 3) for WT (black) or *gyrA*<sup>r</sup> single mutant (blue) treated with ciprofloxacin concentrations resulting in ~40% growth inhibition (condition ii from Fig. 6). \*, P < 0.05, unpaired t test. (B) Location of DNA damage/SOS response genes induced in *gyrA*<sup>r</sup> single-mutant strain. x axis indicates gene position along the *A. baumannii* chromosome, and y axis indicates the log<sub>2</sub> fold change (1.1 μg/ml Cip versus untreated, *gyrA*<sup>r</sup> single mutant) from previously presented RNA-seq data. (C) Population fluorescence analysis of *recA* reporter induction from a representative experiment. Strains of the indicated genotype harboring pCC1 (*recA-mKate2*) were cultured with or without ciprofloxacin as in RNA-seq experiments. Top, growth inhibition relative to untreated control was calculated. Bottom, mKate2 intensity per cell was measured by fluorescence microscopy; each data point represents mean mKate2 intensity of a single cell, and bars indicate median values. (D and E) Average inhibition values (top) or average of median fluorescence values (bottom) from multiple independent experiments examining fluorescence reporter levels as in panel C are displayed. Strains of the indicated genotype harbored *recA-mKate2* (D) or pCC7 (*trpB* promoter fused to *mKate2*) (E). Data points represent mean ± SD at each concentration (n ≥ 2). Dotted lines denote average fluorescence intensity of untreated samples. (F) Rifampin resistance mutation frequency in WT or *gyrA*<sup>r</sup> mutant strains grown in the absence or presence of the indicated ciprofloxacin dose for 3 h. Data points show the efficiency of colony formation on LB agar plates containing rifampin compared to LB agar without antibiotic from n = 4 independent experiments. \*, P = 0.032, unpaired t test.

reporter fusion were cultured in the presence of graded levels of ciprofloxacin, and reporter signal was measured in individual cells by fluorescence microscopy (see Materials and Methods). Increasing sub-MIC doses of ciprofloxacin caused increasing degrees of induction of the *recA* reporter in all strain backgrounds (Fig. 7C and D). Notably, reporter activity was approximately 2-fold higher in the *gyrA*<sup>r</sup> single mutant than in the WT or double mutant at equivalent levels of growth inhibition (Fig. 7C and D). Various degrees of *recA* induction within populations of *gyrA*<sup>r</sup> single-mutant cells

were observed, and this variability roughly matched that observed with WT (Fig. 7C and S4). Increased signal in the *gyrA<sup>r</sup>* mutant strain was not observed with a control reporter fusion to a gene that is nonresponsive to ciprofloxacin (*trpBp*-UTR [45]) (Fig. 7D), indicating that the SOS transcriptional response was specifically enhanced as a consequence of ciprofloxacin inhibition of topo IV.

We hypothesized that the enhanced ciprofloxacin-induced SOS response in the *gyrA<sup>r</sup>* single-mutant strain leads to increased mutagenesis. To measure mutagenesis levels, we calculated the frequency of rifampin-resistant mutants in cultures of WT or *gyrA<sup>r</sup>* mutant after 3 h of growth in the absence or presence of sub-MIC ciprofloxacin doses that result in 10 to 15% growth inhibition (see Materials and Methods). The *gyrA<sup>r</sup>* mutant bacteria exposed to ciprofloxacin showed a higher frequency of rifampin-resistant mutants than when strains were untreated or than the ciprofloxacin-treated WT (Fig. 7E). Together with the observation that *umuC* and *umuD* genes encoding low-fidelity DNA polymerase V show enhanced induction in *gyrA<sup>r</sup>* mutant cells compared to the WT or *gyrA<sup>r</sup> parC<sup>r</sup>* mutant strain (Fig. 7A), these findings are consistent with the model that the enhanced SOS response resulting from ciprofloxacin inhibition of topo IV is linked to a higher frequency of mutagenesis in the *gyrA<sup>r</sup>* single mutant.

## DISCUSSION

In this study, we exploited the dual-target nature of fluoroquinolone antibiotics to uncover how resistance alleles acquired in target enzymes modulate the landscape of intrinsic resistance and transcriptional responses to this class of drug. Using Tn-seq, we performed comprehensive screens for determinants of altered sensitivity to the fluoroquinolone drug ciprofloxacin in isogenic *A. baumannii* strains in which the drug preferentially targets either DNA gyrase or topo IV. We found that the spectra of genes contributing to intrinsic resistance were similar in genetic backgrounds in which both enzymes were WT or in which both enzymes had lowered drug sensitivity due to well-known acquired point mutations. Intrinsic resistance determinants identified in both backgrounds included the AdeIJK and AbeM efflux pumps, multiple subunits of the DNA recombination and repair machinery, a periplasmic protease CtpA, the cell wall transpeptidase PBP1A, and several proteins of unknown function. In contrast, the interaction of ciprofloxacin with the *gyrA<sup>r</sup>* single mutant in which topo IV is the sensitive target dramatically altered the profile of genes that influence relative Tn-seq fitness. This altered fitness profile in *gyrA<sup>r</sup> parC<sup>+</sup>* mutant bacteria was shown to directly reflect the amplification of DNA in the vicinity of two endogenous prophages due to preferential poisoning of topo IV by ciprofloxacin. This study highlights the potential for specific genotype-condition interactions to create unexpected chromosome positional bias in Tn-seq fitness analysis (46). Prophage transcripts and the SOS pathway were also hyperactivated as a consequence of topo IV poisoning by ciprofloxacin, likely facilitating the initiation of synthesis of prophage DNA in the *gyrA<sup>r</sup>* mutant strain.

Our data can be explained by the model shown in Fig. 8, if we assume that reactivation of *A. baumannii* prophages 1 and 3 requires the function of host DNA gyrase. In the WT and the *gyrA<sup>r</sup> parC<sup>r</sup>* double mutant, DNA gyrase is the effective target blocked by ciprofloxacin at growth-inhibitory sub-MIC drug concentrations. Prophage DNA synthesis is inefficient despite induction of the DNA damage response and prophage gene transcription because, as postulated by the model, efficient replication of the prophage genomes requires functional host gyrase (Fig. 8A and C). In contrast, in *gyrA<sup>r</sup>* mutant bacteria, topo IV is the preferred target of intoxication by ciprofloxacin. This interaction causes DNA lesions that robustly stimulate the SOS pathway and prophage transcription; further, host DNA gyrase is available to facilitate efficient prophage genome replication because the GyrA(S81L) (*gyrA<sup>r</sup>*) variant is resistant to the intermediate concentrations of ciprofloxacin required for topo IV poisoning (Fig. 8B).

The central assumption of the model is plausible based on analogy with several other bacteriophage systems that have been shown to require host DNA gyrase for replication. Gyrase inhibitors (quinolones or aminocoumarins) inhibit phage DNA replication during lytic growth after infection (47–52) and disrupt induction of replicative

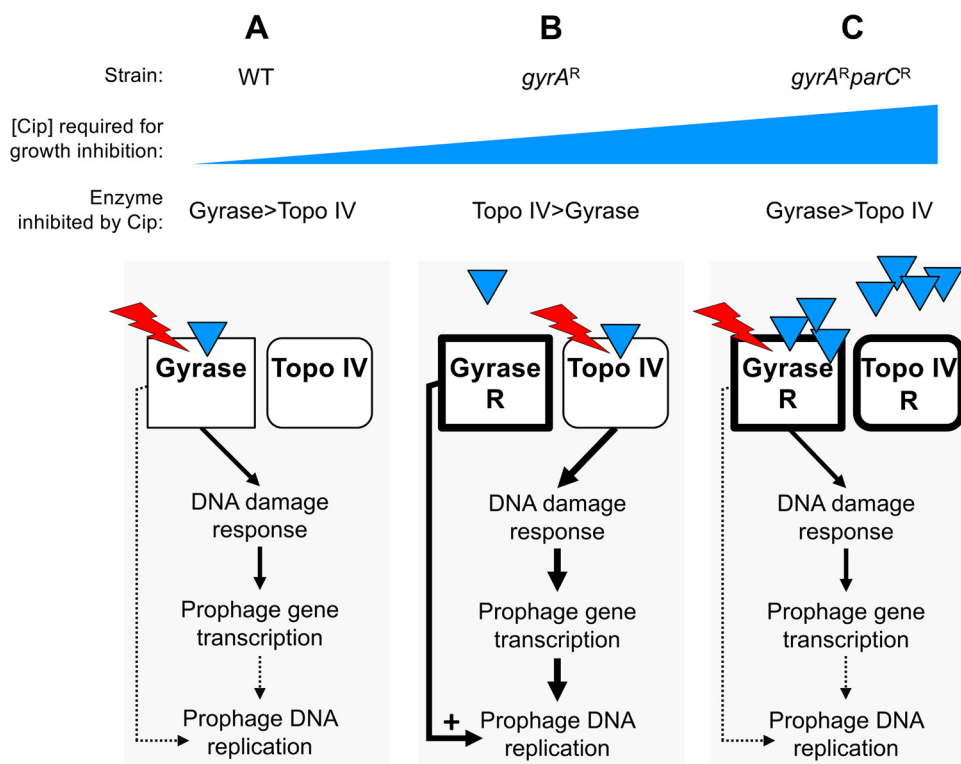


**FIG 8** Model for resistance allele-dependent prophage amplification in *A. baumannii* exposed to sub-MIC fluoroquinolone stress. The model posits that prophage DNA replication depends on host DNA gyrase activity. (A) In WT cells, both gyrase (GyrA) and topo IV (ParC) are drug sensitive. Gyrase, which has higher affinity for ciprofloxacin (blue triangles), is effectively targeted by the drug. Ciprofloxacin-corrupted gyrase enzyme, indicated by red lightning symbol, results in double-strand DNA breaks that signal derepression of prophage gene expression. Prophage DNA replication cannot proceed efficiently, however, because gyrase function is blocked. (B) In *gyrA<sup>R</sup>* single mutant cells, topo IV/ParC has higher affinity for ciprofloxacin than does the resistant gyrase and is the effective drug target. Topo IV corruption results in a robust DNA damage response and activation of prophage gene expression, and gyrase-dependent prophage replication (prophages 1 and 3) proceeds efficiently because GyrA is not drug inhibited. (C) In *gyrA<sup>R</sup> parC<sup>R</sup>* double-mutant cells growing at high drug concentrations, GyrA again has relatively higher affinity for ciprofloxacin than does ParC and becomes the effective target despite the S81L drug binding site alteration. The resulting DNA lesions induce the SOS response and prophage gene expression, but prophage replication does not proceed efficiently because gyrase function is again blocked.

transposition in Mu lysogens (53). Moreover, host gyrase is required for propagation of replication forks within supercoiled DNA substrates in reconstituted systems modeling phage lambda replication (54, 55). The importance of this enzyme class for replication of *A. baumannii* strain 17978 prophages is emphasized by the fact that they do not encode type II topoisomerases which are often encoded by bacteriophages to bypass a requirement for the host enzymes (56, 57).

An alternative model is that at the sub-MIC drug doses resulting in equivalent growth inhibition, gyrase poisoning results in DNA lesions that do not stimulate the SOS response above the threshold required for efficient prophage induction, in contrast to lesions caused by topo IV poisoning. Arguing against this model are the observations that transcription of the SOS response gene *recA* and genes from all three prophages are strongly induced (25- to 50-fold, Fig. 6B and 7C and D) above baseline in WT cells, and Tn-seq fitness results showing the relatively similar importance of DNA damage repair enzymes across all strain backgrounds (Data Sets S1 to S3). We showed that topo IV intoxication stimulated the SOS pathway to a greater extent than that caused by gyrase poisoning, potentially contributing to the robust activation of prophages. This is consistent with previous findings that topo IV and gyrase intoxication can be distinguished by several characteristics. Topo IV lesions result in slower inhibition of DNA synthesis and are thought to be more readily reversed by recombinational repair, resulting in lower cytotoxicity at given drug concentrations (16). These less toxic lesions

could potentially expose more numerous or potent signals for the SOS response that could result in prophage induction.

In contrast to the induction of prophages 1 and 3, ciprofloxacin-induced DNA replication was not observed with prophage 2 despite activation of prophage gene transcription. One possible explanation is that prophage 2 is defective for DNA replication. We consider this unlikely because transposon insertions were unobtainable in a phage locus (ACX60\_RS10145) encoding a putative Cro/C1 family repressor (Data Sets S1 to S3), indicating that this prophage has the potential for lytic replication in the absence of a protein controlling lysogeny maintenance. Consistent with the potential of all three prophages (including P2) for replication, mobilized DNA corresponding to each of the three prophages was detected in phage particles resulting from treatment of WT *A. baumannii* 17978 with mitomycin C, which damages DNA directly without dependence on interactions with DNA topoisomerases (44). An alternative explanation for the lack of prophage 2 DNA amplification observed with fluoroquinolone treatment in our study is that its replication depends on both DNA gyrase and topo IV.

The findings described here have implications for the evolution of antibiotic resistance in *A. baumannii* and potentially other organisms. They indicate that in the trajectory toward high-level fluoroquinolone resistance and intermediate states with moderate-level fluoroquinolone resistance (exemplified by the *gyrA*<sup>r</sup> single mutant) are those that possess highest potential for prophage induction and mutagenesis during growth with continued drug exposure. This could influence how additional drug resistance alleles are acquired. Acquisition of the subsequent *parC* mutation resulting in high-level fluoroquinolone resistance would reset the proclivity for enhanced drug-induced SOS response and prophage amplification. It is notable that hyperamplified and hyperexpressed DNA in the *gyrA*<sup>r</sup> single mutant includes multiple *umuC* and *umuD* paralogs encoding mutagenic DNA polymerases (Fig. 7A and B) (58), whose higher levels could potentially influence adaptation in bacterial populations during drug treatment. Moreover, these findings raise the possibility of enhanced horizontal transfer of phage-associated and phage-proximal genes as a consequence of fluoroquinolone-*gyrA*<sup>r</sup> mutant interactions. Prophage clusters with sequence homology to P1 and P3 prophages exist in additional *A. baumannii* isolates, and in other isolates more divergent prophages can be found at identical chromosomal locations (59). Therefore, the presence of *gyrA*<sup>r</sup> single mutant resistance may broadly modulate how mobile DNA and the *A. baumannii* chromosome respond to fluoroquinolone stress. The relationship between stepwise fluoroquinolone resistance and induction of the SOS response and prophages by this drug class may play out differently with Gram-positive organisms, in which topo IV is typically the sensitive initial target, as opposed to gyrase (6). If the dynamics of fluoroquinolone stress responses in such bacteria have features that accord with the model proposed here, WT strains with two sensitive *parC* and *gyrA* alleles may represent the state with higher potential for drug-induced prophage replication and SOS mutagenesis in Gram-positive organisms compared to derivatives that have acquired single-step target resistance mutations.

In summary, we have demonstrated that in the course of stepwise selection for high drug resistance, intermediate steps result in unexpected modulation of the antibiotic stress response leading to enhanced induction of prophages as well as the enzymatic machinery that drives the acquisition of drug resistance. Future work on analysis of proteins that modulate the survival of drug-resistant mutants should uncover strategies that allow these variants to be targeted therapeutically.

## MATERIALS AND METHODS

**Bacterial strains, growth conditions, and antibiotics.** The bacterial strains used in this work are described in Table S1. *A. baumannii* strains were derivatives of ATCC 17978. Bacterial cultures were grown at 37°C in lysogeny broth (LB; 10 g/liter tryptone, 5 g/liter yeast extract, 10 g/liter NaCl) in flasks with shaking or in tubes on a roller drum. Growth was monitored by measuring absorbance at 600 nm via a spectrophotometer. LB agar was supplemented with antibiotics (ampicillin [Amp], 50 to 100 µg/ml; carbenicillin [Cb], 50 to 100 µg/ml; kanamycin [Km], 10 to 20 µg/ml; amdinocillin; and ciprofloxacin) or sucrose as needed (Sigma-Aldrich).

**Molecular cloning and mutant construction.** The oligonucleotide primers and plasmids used in this study are listed in Table S2. *gyrA*(S81L) (*gyrA'*) and *parC*(S84L) (*parC'*) single point mutations were generated by cloning the respective genomic fragments in pUC18, followed by inverse PCR and self-ligation or amplification and substitution of a mutated gene fragment. In-frame deletions of *adelJK*, *ctpA*, *recN*, and *gidA* were constructed as described previously (60). DNA fragments for deleting prophages P1 and P3 were cloned by PCR amplification of the corresponding *attB* locus and flanking regions from *gyrA'* mutant strains exposed to ciprofloxacin. Constructs were subcloned in pSR47S and used to isolate *A. baumannii* mutants via homologous recombination with two selection steps (60). The *gyrA'* *parC'* double mutant was isolated by selection of a derivative of the *gyrA'* strain able to grow on LB agar containing 8  $\mu\text{g/ml}$  ciprofloxacin. A *pbp1a* mutant (N178TfsX27) was isolated as a derivative of ATCC 17978 selected on LB agar containing 64  $\mu\text{g/ml}$  amdinocillin.

**Antibiotic susceptibility assays.** For growth curve analysis, cultures were seeded at an  $A_{600}$  of 0.003 in 100  $\mu\text{l}$  of broth in wells of a 96-well microtiter plate and growth monitored during incubation at 37°C with orbital shaking in a Tecan M200 Pro plate reader. MIC tests were performed under the conditions described above using serial 2-fold dilutions of drug; the MIC was the lowest drug concentration preventing growth above  $A_{600}$  of 0.05 after 16 h. Colony-forming efficiency in the presence of ciprofloxacin was measured on LB agar plates containing graded concentrations of drug, as previously described (34). For determination of rifampin resistance frequency, bacteria were grown with or without ciprofloxacin for 3 h and pelleted by centrifugation. Dilutions of bacteria were spotted on LB agar to determine the total number of viable bacteria, and remaining bacteria were spread on LB agar plates with 50  $\mu\text{g/ml}$  rifampin to determine rifampin-resistant mutant counts. After overnight incubation at 37°C, the frequency of rifampin mutants was calculated as the CFU per milliliter on LB-rifampin agar plates divided by the CFU per milliliter on LB agar plates.

**Construction of transposon mutant libraries.** Plasmid pDL1073 was employed for transposon mutagenesis. pDL1073 contains a kanamycin-resistant ( $\text{Km}^r$ ) Tn10 derivative, an altered target-specificity Tn10 transposase gene downstream of the phage lambda  $P_L$  promoter, a pSC101ts origin of replication, and  $\beta$ -lactamase (ampicillin resistant [ $\text{Amp}^r$ ]; Fig. S1A). pDL1073 does not replicate in *A. baumannii* at 37°C, allowing efficient detection at this temperature of transposition after delivery via electroporation. *A. baumannii* cells (50  $\mu\text{l}$ ) were combined with 100 ng pDL1073 and electroporated via a Bio-Rad Gene Pulser (0.1-cm-gap-length cuvette; 200 $\Omega$ , 25  $\mu\text{F}$ , and 1.8kV). Electroporated cells were diluted with super optimal broth with catabolite repression (SOC) broth and immediately spread onto membrane filters (0.45- $\mu\text{m}$  pore size) overlaid on prewarmed LB agar plates. After incubating 2 h at 37°C, the filter membranes were transferred to prewarmed LB agar plates containing 20  $\mu\text{g/ml}$  Km and incubated at 37°C overnight to select for transposon mutants. Bacterial colonies were lifted from the filter by agitation in sterile phosphate-buffered saline (PBS). Glycerol was added to 10% (vol/vol), and pooled mutant suspensions were aliquoted and stored at  $-80^\circ\text{C}$ . Eleven to 15 independent pools each consisting of approximately 6,000 to 18,000 mutants were generated in each strain background.

**Tn-seq fitness measurements.** Transposon library aliquots were thawed, vortexed, diluted to an  $A_{600}$  of 0.1, and grown to an  $A_{600}$  of 0.2 in LB. Cultures were then back diluted to  $A_{600}$  of 0.003 in 10 ml LB without drug or with graded concentrations of ciprofloxacin. Parallel cultures were grown at 37°C for approximately 8 generations to an  $A_{600}$  of 0.5 to 1. Samples taken at the start ( $t_1$ ) and end ( $t_2$ ) of this outgrowth were stored at  $-20^\circ\text{C}$ . Eleven to 15 independent transposon libraries were analyzed with each strain background. The use of multiple independent transposon mutant pools and high density of insertions across pools minimizes the contribution of adventitious secondary mutations to the determination of transposon mutant fitness. With WT libraries, treatments with 0.075  $\mu\text{g/ml}$  and 0.09 to 0.1  $\mu\text{g/ml}$  ciprofloxacin were performed in parallel with the same untreated control.

**Tn-seq Illumina library preparation.** Genomic DNA was extracted from  $t_1$  and  $t_2$  samples (Qiagen DNeasy kit) and quantified using a SYBR green microtiter assay. Transposon-adjacent DNA was amplified for Illumina sequencing using a modification of the Nextera DNA library prep method (Illumina). Thirty nanograms of genomic DNA was used as input in a 10- $\mu\text{l}$  tagmentation reaction mixture. The reaction conditions were 55°C for 5 min, followed by inactivation at 95°C for 0.5min. Transposon-adjacent genomic DNA was amplified by adding 40  $\mu\text{l}$  of PCR master mix containing primers olj928 and Nextera 2A-R (0.6  $\mu\text{M}$  final) and Q5 high-fidelity polymerase (NEB). The reaction conditions were 98°C for 10 s, 65°C for 20 s, and 72°C for 1 min (30 cycles), followed by a final extension at 72°C for 2 min. A second PCR was performed using nested indexed primers. This reaction mixture contained 0.5  $\mu\text{l}$  of the first PCR product, Left Tn10 indexing primer (0.6  $\mu\text{M}$ ), Right indexing primer (0.6 $\mu\text{M}$ ), and Q5 polymerase in a 50- $\mu\text{l}$  final volume. The reaction conditions were 12 cycles of 98°C for 10 s, 65°C for 20 s, and 72°C for 1 min, followed by a final extension at 72°C for 2 min. A sample of the second PCR product was imaged after separation on a 2% agarose-Tris-acetate-EDTA (TAE) gel containing SYBR Safe dye. Samples were multiplexed based on signal intensity in the bp 250 to 600 region and purified (Qiagen QIAquick kit). Fifteen to 20 pmol DNA was used as the template in a 50- $\mu\text{l}$  reconditioning reaction mixture containing adapter-specific primers P1 and P2 (0.6  $\mu\text{M}$ ) and Q5 polymerase. The reaction conditions were 95°C for 1 min, 0.1°C/s ramp to 64°C, 64°C for 20 s, and 72°C for 10 min. Samples were purified (Qiagen QIAquick kit), followed by quantification and size selection (250 to 600 bp; Pippin HT) by the Tufts University Genomics Core Facility (TUCF-Genomics). Libraries were sequenced (single-end 50-bp reads) using custom primer olk115 on a HiSeq2500 with high-output V4 chemistry at TUCF-Genomics.

**Tn-seq data analysis.** Reads were demultiplexed, quality filtered, and clipped of adapters before serving as the input for mapping and fitness calculations (31). Reads were mapped to the *A. baumannii* 17978-mff chromosome (GenBank accession number [NZ\\_CP012004](#)) and plasmids (GenBank accession numbers CP000522.1, CP000523.1, and [NZ\\_CP012005](#)) using previously described parameters (61).



Fitness values for each transposon mutant were calculated by comparing mutant versus population-wide expansion between  $t_1$  and  $t_2$  (31). Per-gene average fitness and standard deviation (SD) were then computed from fitness scores for all insertion mutations within a gene across multiple parallel transposon pools. Differences in average gene fitness between treated and untreated conditions ( $W_{diff}$ ) were considered significant if they fulfilled the following 3 criteria, with minor modifications from those previously described (33): per-gene fitness must be calculated from at least 3 data points, the magnitude of  $W_{diff}$  must be  $>10\%$ , and the  $q$  value must be  $<0.05$  in an unpaired  $t$  test, with FDR controlled by the 2-stage step-up method of Benjamini, Krieger, and Yekutieli (GraphPad Prism 7) (69). Per-insertion fitness scores within a given genomic region were visualized using the Integrative Genomics Viewer software (62) after aggregating all scores across multiple independent transposon mutant libraries using the SingleFitness Perl script (63).

**Whole-genome sequencing of individual strains subjected to ciprofloxacin.** WT, *gyrA<sup>r</sup>* mutant, and *gyrA<sup>r</sup> parC<sup>r</sup>* mutant strains were grown from single colonies to early postexponential phase and back diluted to an  $A_{600}$  of 0.003. Parallel cultures were grown for 2.5 h in the absence of treatment or 3.5 h in the presence of ciprofloxacin treatment. DNA was extracted (Qiagen DNeasy kit), and Illumina sequencing libraries were amplified and sequenced as described previously (34). After mapping to [NZ\\_CP012004](#), coverage files were generated from the resulting BAM files using deepTools, with reads normalized to counts per million (64).

**Transcriptional profiling.** Cultures were diluted to an  $A_{600}$  of 0.003 and grown for 2.5 h (untreated) or 3.5 h (ciprofloxacin treated). Cultures were mixed with an equal volume of ice-cold acetone-ethanol (1:1) and stored at  $-80^{\circ}\text{C}$ . Cells were thawed and washed with Tris-EDTA (TE), and RNA was extracted (Qiagen RNeasy kit). RNA samples were diluted, combined with SUPERase-in (Invitrogen), and processed via the RNAtag-seq method (42). Illumina cDNA sequencing libraries were sequenced and reads processed as described previously (65). Differential expression was calculated using DESeq2 (66).

**Fluorescence reporter assays.** Strains containing pCC1 or pCC7 were cultured in the presence or absence of ciprofloxacin as in the RNA-seq experiments. Cells were immobilized on agarose pads and imaged on a Leica AF6000 microscope using a  $100\times/1.3$  objective and TX2 filter cube (excitation, band pass [BP] 560/40; dichromatic mirror, 595; emission, BP 645/75). MicroBeJ (67) was used to measure the background-corrected mean fluorescence intensity per cell. Median cellular fluorescence intensities from populations of at least 100 bacteria were determined, and median values across multiple independent experiments were averaged.

**Data availability.** The sequencing reads analyzed in this study were deposited in the SRA database under accession number [SRP157243](#) (Tn-seq) and BioProject numbers [PRJNA495614](#) (RNA-seq) and [PRJNA495623](#) (whole-genome sequencing).

## SUPPLEMENTAL MATERIAL

Supplemental material for this article may be found at <https://doi.org/10.1128/mBio.01127-19>.

**FIG S1**, PDF file, 0.2 MB.

**FIG S2**, PDF file, 0.7 MB.

**FIG S3**, PDF file, 0.1 MB.

**FIG S4**, PDF file, 0.1 MB.

**TABLE S1**, PDF file, 0.1 MB.

**TABLE S2**, PDF file, 0.1 MB.

**DATA SET S1**, XLSX file, 2 MB.

**DATA SET S2**, XLSX file, 0.8 MB.

**DATA SET S3**, XLSX file, 0.8 MB.

**DATA SET S4**, XLSX file, 2.3 MB.

## ACKNOWLEDGMENTS

This work was supported by NIAID awards U01AI124302 to R.R.I. and T.V.O., R21AI128328 to R.R.I., and F32AI098358 to E.G. NSF REU Site award 1757443 to the Northeastern University Department of Biology supported the research of E.L.W.

We thank Carly Ching and Veronica Godoy for the gifts of pCC1 and pCC7 and Amy Tang for assistance with bioinformatics analysis.

## REFERENCES

1. Tacconelli E, Carrara E, Savoldi A, Harbarth S, Mendelson M, Monnet DL, Pulcini C, Kahlmeter G, Kluytmans J, Carmeli Y, Oueltte M, Outterson K, Patel J, Cavalieri M, Cox EM, Houchens CR, Grayson ML, Hansen P, Singh N, Theuretzbacher U, Magrini N, WHO Pathogens Priority List Working Group. 2018. Discovery, research, and development of new antibiotics: the WHO priority list of antibiotic-resistant bacteria and tuberculosis. *Lancet Infect Dis* 18:318–327. [https://doi.org/10.1016/S1473-3099\(17\)30753-3](https://doi.org/10.1016/S1473-3099(17)30753-3).
2. Warner WA, Kuang SN, Hernandez R, Chong MC, Ewing PJ, Fleischer J, Meng J, Chu S, Terashita D, English L, Chen W, Xu HH. 2016. Molecular characterization and antimicrobial susceptibility of *Acinetobacter baumannii* isolates obtained from two hospital outbreaks in Los Angeles

- County, California, USA. *BMC Infect Dis* 16:194. <https://doi.org/10.1186/s12879-016-1526-y>.
3. Kim D, Ahn JY, Lee CH, Jang SJ, Lee H, Yong D, Jeong SH, Lee K. 2017. Increasing resistance to extended-spectrum cephalosporins, fluoroquinolone, and carbapenem in Gram-negative bacilli and the emergence of carbapenem non-susceptibility in *Klebsiella pneumoniae*: analysis of Korean Antimicrobial Resistance Monitoring System (KARMS) data from 2013 to 2015. *Ann Lab Med* 37:231–239. <https://doi.org/10.3343/alm.2017.37.3.231>.
  4. Blanco N, Harris AD, Rock C, Johnson JK, Pineles L, Bonomo RA, Srinivasan A, Pettigrew MM, Thom KA, the CDC Epicenters Program. 2018. Risk factors and outcomes associated with multidrug-resistant *Acinetobacter baumannii* upon intensive care unit admission. *Antimicrob Agents Chemother* 62:e01631-17. <https://doi.org/10.1128/AAC.01631-17>.
  5. Drlica K, Hiasa H, Kerns R, Malik M, Mustaev A, Zhao X. 2009. Quinolones: action and resistance updated. *Curr Top Med Chem* 9:981–998. <https://doi.org/10.2174/156802609789630947>.
  6. Hooper DC. 1999. Mechanisms of fluoroquinolone resistance. *Drug Resist Updat* 2:38–55. <https://doi.org/10.1054/drup.1998.0068>.
  7. Jacoby GA. 2005. Mechanisms of resistance to quinolones. *Clin Infect Dis* 41(Suppl 2):S120–S126. <https://doi.org/10.1086/428052>.
  8. Hujer KM, Hujer AM, Hulten EA, Bajaksouzian S, Adams JM, Donskey CJ, Ecker DJ, Massire C, Eshoo MW, Sampath R, Thomson JM, Rather PN, Craft DW, Fishbain JT, Ewell AJ, Jacobs MR, Paterson DL, Bonomo RA. 2006. Analysis of antibiotic resistance genes in multidrug-resistant *Acinetobacter* sp. isolates from military and civilian patients treated at the Walter Reed Army Medical Center. *Antimicrob Agents Chemother* 50:4114–4123. <https://doi.org/10.1128/AAC.00778-06>.
  9. Valentine SC, Contreras D, Tan S, Real LJ, Chu S, Xu HH. 2008. Phenotypic and molecular characterization of *Acinetobacter baumannii* clinical isolates from nosocomial outbreaks in Los Angeles County, California. *J Clin Microbiol* 46:2499–2507. <https://doi.org/10.1128/JCM.00367-08>.
  10. Fernando D, Zhanel G, Kumar A. 2013. Antibiotic resistance and expression of resistance-nodulation-division pump- and outer membrane porin-encoding genes in *Acinetobacter* species isolated from Canadian hospitals. *Can J Infect Dis Med Microbiol* 24:17–21. <https://doi.org/10.1155/2013/696043>.
  11. Rumbo C, Gato E, López M, Ruiz de Alegría C, Fernández-Cuenca F, Martínez-Martínez L, Vila J, Pachón J, Cisneros JM, Rodríguez-Baño J, Pascual A, Bou G, Tomás M, Spanish Group of Nosocomial Infections and Mechanisms of Action and Resistance to Antimicrobials (GEIH-GEMARA) from the Spanish Society of Clinical Microbiology and Infectious Diseases (SEIMC) and the Spanish Network for Research in Infectious Diseases (REIPI). 2013. Contribution of efflux pumps, porins, and beta-lactamases to multidrug resistance in clinical isolates of *Acinetobacter baumannii*. *Antimicrob Agents Chemother* 57:5247–5257. <https://doi.org/10.1128/AAC.00730-13>.
  12. Yoon EJ, Chabane YN, Goussard S, Snesrud E, Courvalin P, De E, Grillot-Courvalin C. 2015. Contribution of resistance-nodulation-cell division efflux systems to antibiotic resistance and biofilm formation in *Acinetobacter baumannii*. *mBio* 6:e00309-15. <https://doi.org/10.1128/mBio.00309-15>.
  13. Poole K. 2000. Efflux-mediated resistance to fluoroquinolones in Gram-negative bacteria. *Antimicrob Agents Chemother* 44:2233–2241. <https://doi.org/10.1128/aac.44.9.2233-2241.2000>.
  14. Recacha E, Machuca J, Diaz de Alba P, Ramos-Guelfo M, Docobo-Perez F, Rodriguez-Beltran J, Blazquez J, Pascual A, Rodriguez-Martinez JM. 2017. Quinolone resistance reversion by targeting the SOS response. *mBio* 8:e00971-17. <https://doi.org/10.1128/mBio.00971-17>.
  15. Cirz RT, Chin JK, Andes DR, de Crecy-Lagard V, Craig WA, Romesberg FE. 2005. Inhibition of mutation and combating the evolution of antibiotic resistance. *PLoS Biol* 3:e176. <https://doi.org/10.1371/journal.pbio.0030176>.
  16. Khodursky AB, Cozzarelli NR. 1998. The mechanism of inhibition of topoisomerase IV by quinolone antibacterials. *J Biol Chem* 273:27668–27677. <https://doi.org/10.1074/jbc.273.42.27668>.
  17. Mo CY, Manning SA, Roggiani M, Culyba MJ, Samuels AN, Sniogowski PD, Goulian M, Kohli RM. 2016. Systematically altering bacterial SOS Activity under stress reveals therapeutic strategies for potentiating antibiotics. *mSphere* 1:e00163-16. <https://doi.org/10.1128/mSphere.00163-16>.
  18. Nichols RJ, Sen S, Choo YJ, Beltrao P, Zietek M, Chaba R, Lee S, Kazmierczak KM, Lee KJ, Wong A, Shales M, Lovett S, Winkler ME, Krogan NJ, Typas A, Gross CA. 2011. Phenotypic landscape of a bacterial cell. *Cell* 144:143–156. <https://doi.org/10.1016/j.cell.2010.11.052>.
  19. Sutherland JH, Tse-Dinh YC. 2010. Analysis of RuvABC and RecG involvement in the *Escherichia coli* response to the covalent topoisomerase-DNA complex. *J Bacteriol* 192:4445–4451. <https://doi.org/10.1128/JB.00350-10>.
  20. Tamae C, Liu A, Kim K, Sitz D, Hong J, Becket E, Bui A, Solaimani P, Tran KP, Yang H, Miller JH. 2008. Determination of antibiotic hypersensitivity among 4,000 single-gene-knockout mutants of *Escherichia coli*. *J Bacteriol* 190:5981–5988. <https://doi.org/10.1128/JB.01982-07>.
  21. Urios A, Herrera G, Aleixandre V, Blanco M. 1990. Expression of the *recA* gene is reduced in *Escherichia coli* topoisomerase I mutants. *Mutat Res* 243:267–272. [https://doi.org/10.1016/0165-7992\(90\)90142-7](https://doi.org/10.1016/0165-7992(90)90142-7).
  22. Brazas MD, Breidenstein EB, Overhage J, Hancock RE. 2007. Role of Ion, an ATP-dependent protease homolog, in resistance of *Pseudomonas aeruginosa* to ciprofloxacin. *Antimicrob Agents Chemother* 51:4276–4283. <https://doi.org/10.1128/AAC.00830-07>.
  23. Breidenstein EB, Khaira BK, Wiegand I, Overhage J, Hancock RE. 2008. Complex ciprofloxacin resistance revealed by screening a *Pseudomonas aeruginosa* mutant library for altered susceptibility. *Antimicrob Agents Chemother* 52:4486–4491. <https://doi.org/10.1128/AAC.00222-08>.
  24. van Opijnen T, Camilli A. 2012. A fine scale phenotype-genotype virulence map of a bacterial pathogen. *Genome Res* 22:2541–2551. <https://doi.org/10.1101/gr.137430.112>.
  25. Kelley WL. 2006. Lex marks the spot: the virulent side of SOS and a closer look at the LexA regulon. *Mol Microbiol* 62:1228–1238. <https://doi.org/10.1111/j.1365-2958.2006.05444.x>.
  26. Robinson A, Brzoska AJ, Turner KM, Withers R, Harry EJ, Lewis PJ, Dixon NE. 2010. Essential biological processes of an emerging pathogen: DNA replication, transcription, and cell division in *Acinetobacter* spp. *Microbiol Mol Biol Rev* 74:273–297. <https://doi.org/10.1128/MMBR.00048-09>.
  27. MacGuire AE, Ching MC, Diamond BH, Kazakov A, Novichkov P, Godoy VG. 2014. Activation of phenotypic subpopulations in response to ciprofloxacin treatment in *Acinetobacter baumannii*. *Mol Microbiol* 92:138–152. <https://doi.org/10.1111/mmi.12541>.
  28. Aranda J, Bardina C, Beceiro A, Rumbo S, Cabral MP, Barbe J, Bou G. 2011. *Acinetobacter baumannii* RecA protein in repair of DNA damage, antimicrobial resistance, general stress response, and virulence. *J Bacteriol* 193:3740–3747. <https://doi.org/10.1128/JB.00389-11>.
  29. Saroj SD, Clemmer KM, Bonomo RA, Rather PN. 2012. Novel mechanism for fluoroquinolone resistance in *Acinetobacter baumannii*. *Antimicrob Agents Chemother* 56:4955–4957. <https://doi.org/10.1128/AAC.00739-12>.
  30. Gallagher LA, Lee SA, Manoil C. 2017. Importance of core genome functions for an extreme antibiotic resistance trait. *mBio* 8:e01655-17. <https://doi.org/10.1128/mBio.01655-17>.
  31. van Opijnen T, Camilli A. 2013. Transposon insertion sequencing: a new tool for systems-level analysis of microorganisms. *Nat Rev Microbiol* 11:435–442. <https://doi.org/10.1038/nrmicro3033>.
  32. van Opijnen T, Bodi KL, Camilli A. 2009. Tn-seq: high-throughput parallel sequencing for fitness and genetic interaction studies in microorganisms. *Nat Methods* 6:767–772. <https://doi.org/10.1038/nmeth.1377>.
  33. van Opijnen T, Dedrick S, Bento J. 2016. Strain dependent genetic networks for antibiotic-sensitivity in a bacterial pathogen with a large pan-genome. *PLoS Pathog* 12:e1005869. <https://doi.org/10.1371/journal.ppat.1005869>.
  34. Geisinger E, Mortman NJ, Vargas-Cuevas G, Tai AK, Isberg RR. 2018. A global regulatory system links virulence and antibiotic resistance to envelope homeostasis in *Acinetobacter baumannii*. *PLoS Pathog* 14:e1007030. <https://doi.org/10.1371/journal.ppat.1007030>.
  35. Drlica K, Zhao X. 1997. DNA gyrase, topoisomerase IV, and the 4-quinolones. *Microbiol Mol Biol Rev* 61:377–392.
  36. Su XZ, Chen J, Mizushima T, Kuroda T, Tsuchiya T. 2005. AbeM, an H<sup>+</sup>-coupled *Acinetobacter baumannii* multidrug efflux pump belonging to the MATE family of transporters. *Antimicrob Agents Chemother* 49:4362–4364. <https://doi.org/10.1128/AAC.49.10.4362-4364.2005>.
  37. Knauf GA, Cunningham AL, Kazi MI, Riddington IM, Crofts AA, Cattoir V, Trent MS, Davies BW. 2018. Exploring the antimicrobial action of quaternary amines against *Acinetobacter baumannii*. *mBio* 9:e02394-17. <https://doi.org/10.1128/mBio.02394-17>.
  38. Gomez JE, Kaufmann-Malaga BB, Wivagg CN, Kim PB, Silvis MR, Renedo N, Ioerger TR, Ahmad R, Livny J, Fishbein S, Sacchetti JC, Carr SA, Hung DT. 2017. Ribosomal mutations promote the evolution of antibiotic resistance in a multidrug environment. *Elife* 6:e20420. <https://doi.org/10.7554/eLife.20420>.
  39. Bollenbach T, Quan S, Chait R, Kishony R. 2009. Nonoptimal microbial

- response to antibiotics underlies suppressive drug interactions. *Cell* 139:707–718. <https://doi.org/10.1016/j.cell.2009.10.025>.
40. Shippy DC, Fadl AA. 2015. RNA modification enzymes encoded by the gid operon: Implications in biology and virulence of bacteria. *Microb Pathog* 89:100–107. <https://doi.org/10.1016/j.micpath.2015.09.008>.
  41. Hujer KM, Hujer AM, Endimiani A, Thomson JM, Adams MD, Goglin K, Rather PN, Pennella TT, Massire C, Eshoo MW, Sampath R, Blyn LB, Ecker DJ, Bonomo RA. 2009. Rapid determination of quinolone resistance in *Acinetobacter* spp. *J Clin Microbiol* 47:1436–1442. <https://doi.org/10.1128/JCM.02380-08>.
  42. Shishkin AA, Giannoukos G, Kucukural A, Ciulla D, Busby M, Surka C, Chen J, Bhattacharyya RP, Rudy RF, Patel MM, Novod N, Hung DT, Gnirke A, Garber M, Guttman M, Livny J. 2015. Simultaneous generation of many RNA-seq libraries in a single reaction. *Nat Methods* 12:323–325. <https://doi.org/10.1038/nmeth.3313>.
  43. Simmons LA, Foti JJ, Cohen SE, Walker GC. 2008. The SOS regulatory network. *EcoSal Plus* 3. <https://doi.org/10.1128/ecosalplus.5.4.3>.
  44. Hare JM, Ferrell JC, Witkowski TA, Grice AN. 2014. Prophage induction and differential RecA and UmuDAB transcriptome regulation in the DNA damage responses of *Acinetobacter baumannii* and *Acinetobacter baylyi*. *PLoS One* 9:e93861. <https://doi.org/10.1371/journal.pone.0093861>.
  45. Ching C, Gozzi K, Heinemann B, Chai Y, Godoy VG. 2017. RNA-mediated cis regulation in *Acinetobacter baumannii* modulates stress-induced phenotypic variation. *J Bacteriol* 199:e00799-16. <https://doi.org/10.1128/JB.00799-16>.
  46. Chao MC, Abel S, Davis BM, Waldor MK. 2016. The design and analysis of transposon insertion sequencing experiments. *Nat Rev Microbiol* 14:119–128. <https://doi.org/10.1038/nrmicro.2015.7>.
  47. Erb ML, Kraemer JA, Coker JK, Chaikeratisak V, Nonejuie P, Agard DA, Pogliano J. 2014. A bacteriophage tubulin harnesses dynamic instability to center DNA in infected cells. *Elife* 3. <https://doi.org/10.7554/eLife.03197>.
  48. Constantinou A, Voelkel-Meiman K, Sternglanz R, McCorquodale MM, McCorquodale DJ. 1986. Involvement of host DNA gyrase in growth of bacteriophage T5. *J Virol* 57:875–882.
  49. Alonso JC, Sarachu AN, Grau O. 1981. DNA gyrase inhibitors block development of *Bacillus subtilis* bacteriophage SP01. *J Virol* 39:855–860.
  50. Alcorlo M, Salas M, Hermoso JM. 2007. In vivo DNA binding of bacteriophage GA-1 protein p6. *J Bacteriol* 189:8024–8033. <https://doi.org/10.1128/JB.01047-07>.
  51. Kreuzer KN, Cozzarelli NR. 1979. *Escherichia coli* mutants thermosensitive for deoxyribonucleic acid gyrase subunit A: effects on deoxyribonucleic acid replication, transcription, and bacteriophage growth. *J Bacteriol* 140:424–435.
  52. Itoh T, Tomizawa JI. 1977. Involvement of DNA gyrase in bacteriophage T7 DNA replication. *Nature* 270:78–80. <https://doi.org/10.1038/270078a0>.
  53. Sokolsky TD, Baker TA. 2003. DNA gyrase requirements distinguish the alternate pathways of Mu transposition. *Mol Microbiol* 47:397–409. <https://doi.org/10.1046/j.1365-2958.2003.03296.x>.
  54. Dodson M, Echols H, Wickner S, Alfano C, Mensa-Wilmot K, Gomes B, LeBowitz J, Roberts JD, McMacken R. 1986. Specialized nucleoprotein structures at the origin of replication of bacteriophage lambda: localized unwinding of duplex DNA by a six-protein reaction. *Proc Natl Acad Sci U S A* 83:7638–7642. <https://doi.org/10.1073/pnas.83.20.7638>.
  55. Mensa-Wilmot K, Seaby R, Alfano C, Wold MC, Gomes B, McMacken R. 1989. Reconstitution of a nine-protein system that initiates bacteriophage lambda DNA replication. *J Biol Chem* 264:2853–2861.
  56. Kreuzer KN. 1998. Bacteriophage T4, a model system for understanding the mechanism of type II topoisomerase inhibitors. *Biochim Biophys Acta* 1400:339–347. [https://doi.org/10.1016/S0167-4781\(98\)00145-6](https://doi.org/10.1016/S0167-4781(98)00145-6).
  57. Huang WM, Wei LS, Casjens S. 1985. Relationship between bacteriophage T4 and T6 DNA topoisomerases. T6 39-protein subunit is equivalent to the combined T4 39- and 60-protein subunits. *J Biol Chem* 260:8973–8977.
  58. Sutton MD, Smith BT, Godoy VG, Walker GC. 2000. The SOS response: recent insights into umuDC-dependent mutagenesis and DNA damage tolerance. *Annu Rev Genet* 34:479–497. <https://doi.org/10.1146/annurev.genet.34.1.479>.
  59. Di Nocera PP, Rocco F, Giannouli M, Triassi M, Zarrilli R. 2011. Genome organization of epidemic *Acinetobacter baumannii* strains. *BMC Microbiol* 11:224. <https://doi.org/10.1186/1471-2180-11-224>.
  60. Geisinger E, Isberg RR. 2015. Antibiotic modulation of capsular exopolysaccharide and virulence in *Acinetobacter baumannii*. *PLoS Pathog* 11:e1004691. <https://doi.org/10.1371/journal.ppat.1004691>.
  61. Carter R, Wolf J, van Opijnen T, Muller M, Obert C, Burnham C, Mann B, Li Y, Hayden RT, Pestina T, Persons D, Camilli A, Flynn PM, Tuomanen EI, Rosch JW. 2014. Genomic analyses of pneumococci from children with sickle cell disease expose host-specific bacterial adaptations and deficits in current interventions. *Cell Host Microbe* 15:587–599. <https://doi.org/10.1016/j.chom.2014.04.005>.
  62. Robinson JT, Thorvaldsdottir H, Winckler W, Guttman M, Lander ES, Getz G, Mesirov JP. 2011. Integrative genomics viewer. *Nat Biotechnol* 29:24–26. <https://doi.org/10.1038/nbt.1754>.
  63. McCoy KM, Antonio ML, van Opijnen T. 2017. MAGenTA: a Galaxy implemented tool for complete Tn-Seq analysis and data visualization. *Bioinformatics* 33:2781–2783. <https://doi.org/10.1093/bioinformatics/btx320>.
  64. Ramirez F, Dundar F, Diehl S, Gruning BA, Manke T. 2014. deepTools: a flexible platform for exploring deep-sequencing data. *Nucleic Acids Res* 42:W187–W191. <https://doi.org/10.1093/nar/gku365>.
  65. Jensen PA, Zhu Z, van Opijnen T. 2017. Antibiotics disrupt coordination between transcriptional and phenotypic stress responses in pathogenic bacteria. *Cell Rep* 20:1705–1716. <https://doi.org/10.1016/j.celrep.2017.07.062>.
  66. Love MI, Huber W, Anders S. 2014. Moderated estimation of fold change and dispersion for RNA-seq data with DESeq2. *Genome Biol* 15:550. <https://doi.org/10.1186/s13059-014-0550-8>.
  67. Ducret A, Quardokus EM, Brun YV. 2016. MicrobeJ, a tool for high throughput bacterial cell detection and quantitative analysis. *Nat Microbiol* 1:16077. <https://doi.org/10.1038/nmicrobiol.2016.77>.
  68. Arndt D, Grant JR, Marcu A, Sajed T, Pon A, Liang Y, Wishart DS. 2016. PHASTER: a better, faster version of the PHAST phage search tool. *Nucleic Acids Res* 44:W16–W21. <https://doi.org/10.1093/nar/gkw387>.
  69. Benjamini Y, Krieger AM, Yekutieli D. 2006. Adaptive linear step-up procedures that control the false discovery rate. *Biometrika* 93:491–507. <https://doi.org/10.1093/biomet/93.3.491>.